The EMBO Journal (2004) 23, 212–220 | © 2004 European Molecular Biology Organization | All Rights Reserved 0261-4189/04
www.embojournal.org

THE EMBO JOURNAL

Akt negatively regulates the *in vitro* lifespan of human endothelial cells via a p53/p21-dependent pathway

Hideyuki Miyauchi[1], Tohru Minamino[1], Kaoru Tateno, Takeshige Kunieda, Haruhiro Toko and Issei Komuro*

Department of Cardiovascular Science and Medicine, Chiba University Graduate School of Medicine, Chuo-ku, Chiba, Japan

The signaling pathway of insulin/insulin-like growth factor-1/phosphatidylinositol-3 kinase/Akt is known to regulate longevity as well as resistance to oxidative stress in the nematode *Caenorhabditis elegans*. This regulatory process involves the activity of DAF-16, a forkhead transcription factor. Although reduction-of-function mutations in components of this pathway have been shown to extend the lifespan in organisms ranging from yeast to mice, activation of Akt has been reported to promote proliferation and survival of mammalian cells. Here we show that Akt activity increases along with cellular senescence and that inhibition of Akt extends the lifespan of primary cultured human endothelial cells. Constitutive activation of Akt promotes senescence-like arrest of cell growth via a p53/p21-dependent pathway, and inhibition of forkhead transcription factor FOXO3a by Akt is essential for this growth arrest to occur. FOXO3a influences p53 activity by regulating the level of reactive oxygen species. These findings reveal a novel role of Akt in regulating the cellular lifespan and suggest that the mechanism of longevity is conserved in primary cultured human cells and that Akt-induced senescence may be involved in vascular pathophysiology.

The EMBO Journal (2004) **23**, 212–220. doi:10.1038/sj.emboj.7600045; Published online 8 January 2004
Subject Categories: cell cycle; molecular biology of disease
Keywords: aging; Akt; endothelial cells; senescence

Introduction

Cellular senescence is the limited ability of primary human cells to divide when cultured *in vitro* and is accompanied by a specific set of changes in cell morphology, gene expression and function. These phenotypic changes have been implicated in human aging (Faragher and Kipling, 1998). This hypothesis, the cellular hypothesis of aging, was established by Hayflick (1975) and is supported by evidence that the replicative potential of primary cultured human cells is dependent on donor age and that the growth potential of cultured cells correlates well with the mean maximum lifespan of the species from which the cells are derived (Rohme, 1981), although some conflicting data have been reported (Cristofalo *et al*, 1998). Primary cultured cells obtained from patients with premature aging syndromes, such as Werner syndrome and Bloom syndrome, are known to have a shorter lifespan than the cells from age-matched healthy populations (Rohme, 1981; Thompson and Holliday, 1983), further supporting this hypothesis. Cell division is essential for the survival of multicellular organisms that contain renewable tissues, but also places the organism at the risk of developing cancer. It has been suggested that complex organisms have evolved at least two cellular mechanisms to prevent oncogenic transformation, which are apoptosis and cellular senescence (Campisi, 2001). Accordingly, age-associated diseases could be regarded as a by-product of the tumor suppressor mechanism, cellular senescence (Weinstein and Ciszek, 2002).

Many molecular mechanisms have been suggested to contribute to human aging and its associated diseases. Recent genetic analyses have demonstrated that reduction-of-function mutations in the signaling pathway of insulin/insulin-like growth factor-1 (IGF-1)/phosphatidylinositol-3 kinase (PI3K)/Akt (also known as protein kinase B) extend the longevity of the nematode *Caenorhabditis elegans* (Kenyon *et al*, 1993; Morris *et al*, 1996; Paradis and Ruvkun, 1998; Guarente and Kenyon, 2000; Kenyon, 2001; Lee *et al*, 2001; Lin *et al*, 2001; Longo and Finch, 2003). The forkhead transcription factor DAF-16, which is phosphorylated and thereby inactivated by Akt (Lee *et al*, 2001; Lin *et al*, 2001), plays an essential role in this longevity pathway (Lin *et al*, 1997; Ogg *et al*, 1997). More recently, it has been reported that the genes regulating longevity are conserved in organisms ranging from yeast to mice. Mutation of *Sch9*, which is homologous to *Akt*, extends the lifespan of yeast (Fabrizio *et al*, 2001), and mutations that decrease the activity of the insulin/IGF-1-like pathway increase the longevity of fruit flies (Tatar *et al*, 2001) and mice (Bluher *et al*, 2003; Holzenberger *et al*, 2003). These mutations that extend the lifespan are associated with increased resistance to oxidative stress, which is partly mediated by the increased expression of antioxidant genes (Honda and Honda, 1999; Fabrizio *et al*, 2003; Murphy *et al*, 2003).

In mammalian cells, activation of Akt has been reported to induce proliferation and survival, thereby promoting tumorigenesis (Datta *et al*, 1999; Blume-Jensen and Hunter, 2001; Testa and Bellacosa, 2001). Overexpression of Akt can transform NIH3T3 cells (Cheng *et al*, 1997), while introduction of Akt antisense RNA inhibits the tumorigenic phenotype of cancer cells expressing high levels of Akt (Cheng *et al*, 1996). The mechanisms by which Akt promotes cell proliferation and survival are likely to be multifactorial, because it has been reported to directly phosphorylate several components of the cell cycle machinery as well as the cell death machinery (Datta *et al*, 1999). Akt counteracts the effect of

*Corresponding author. Department of Cardiovascular Science and Medicine, Chiba University Graduate School of Medicine, 1-8-1 Inohana, Chuo-ku, Chiba 260-8670, Japan. Tel.: +81 43 226 2097; Fax: +81 43 226 2557; E-mail: komuro-tky@umin.ac.jp
[1]These authors contributed equally to this work

Received: 25 June 2003; accepted: 25 November 2003; Published online: 8 January 2004

©2004 European Molecular Biology Organization

cyclin-dependent kinase inhibitors on cell cycle progression by modulating their intracellular localization and level of transcription (Medema *et al*, 2000; Shin *et al*, 2002; Viglietto *et al*, 2002; Zhou *et al*, 2001a). Akt also increases the cyclin D1 level by inhibiting its degradation, which is important in the G1/S phase transition (Diehl *et al*, 1998). Moreover, it is known that Akt phosphorylates and inactivates proapoptotic factors such as BAD (Datta *et al*, 1997; del Peso *et al*, 1997) and procaspase-9 (Cardone *et al*, 1998), thereby promoting cell survival. Although these reports have suggested an important role of Akt in human malignancy (Blume-Jensen and Hunter, 2001; Testa and Bellacosa, 2001), it has mainly been examined in immortal cell lines and the impact of Akt activation on the growth and lifespan of primary cultured human cells is unknown.

In the present study, we found that inhibition of Akt could prolong the lifespan of primary cultured human endothelial cells, whereas constitutive activation of Akt promoted senescence-like growth arrest via a p53/p21-dependent pathway. Akt-induced growth arrest was inhibited by a mutated forkhead transcription factor that was resistant to Akt phosphorylation. These findings disclose a novel role of Akt in regulating the lifespan of cells and suggest that the mechanism of longevity is conserved in primary cultured human cells.

Results

Akt activation reduces the lifespan of human endothelial cells

We first investigated whether Akt activity was associated with cellular senescence of primary cultured human endothelial cells. Senescent endothelial cells had higher phospho-Akt levels than young endothelial cells (Figure 1A). To assess the actual role of Akt activity in regulating cellular lifespan, we infected primary cultured human endothelial cells with a retroviral vector encoding either constitutively activated myc-tagged Akt (AktCA) or dominant-negative myc-tagged Akt (AktDN). The empty retroviral vector pLNCX (Mock), encoding a neomycin resistance gene alone, was also transduced into endothelial cells as a control. Infected cells were purified using G418 for 7 days and then recultured until the cells underwent senescence. The 8th day after infection is designated as day 0 in all of the following experiments. Western blot analysis with anti-c-Myc antibody and anti-Akt antibody demonstrated that both AktCA and AktDN proteins were expressed by the endothelial cells, showing an approximately 4- to 8-fold increase of total Akt protein compared to endogenous Akt protein (Figure 1B). Long-term culture studies showed that constitutive activation of Akt significantly shortened the lifespan of the endothelial cells, whereas inhibition of Akt activity delayed senescence compared with mock-infected cells (Figure 1B). Introduction of AktDN influenced cellular lifespan in the late passages, but not in the early passages, suggesting that Akt activity increased with further cell division and thus promoted senescence. Expression of AktCA markedly reduced cell growth by day 7 (Figure 1C). AktCA-transduced endothelial cells were flattened and enlarged, while mock- or AktDN-infected endothelial cells exhibited normal morphology and growth (Figures 1C and D). Senescence-associated β-galactosidase activity was also increased in AktCA-transduced cells (Figure 1D). These changes of the phenotype, which were suggestive of senescence, were observed in various types of endothelial cells including microvascular endothelial cells (Supplementary Figure 1). The same senescence-like changes also occurred in confluent endothelial cells (Supplementary Figure 2). Thus, constitutive activation of Akt induced a senescence-like phenotype in human endothelial cells irrespective of the cell type and growth pattern. To further explore the relationship between Akt activity and cell growth, we isolated clones from AktCA-infected endothelial cells and determined the phospho-Akt level and the cell number on day 30. Clones obtained from mock-infected cell populations could be expanded up to $1–3 \times 10^6$ cells on average and revealed little Akt activity (Figure 1E, lane 1). In contrast, most of the AktCA-infected clones showed almost complete growth arrest and high levels of phospho-Akt expression (Figure 1E, lanes 5–7). However, some AktCA-infected clones showed low phospho-Akt levels and continued to proliferate (Figure 1E, lanes 2–4). Such proliferating populations may lead to underestimation of the growth inhibitory effect of AktCA in long-term culture experiments. The level of phospho-Akt was inversely correlated with the number of cells on day 30 (Figure 1E, right graph). Thus, we concluded that Akt is a negative regulator of the lifespan of primary cultured human endothelial cells.

Upregulation of p21 is essential for Akt-induced growth arrest

To clarify the mechanism of cell growth arrest induced by activation of Akt, we examined the expression of cell cycle regulatory proteins. Expression of p53 and $p21^{Waf1/Cip1}$, but not $p16^{Ink4a}$, was elevated, while the level of phosphorylated Rb was decreased in AktCA-infected cells compared with mock-infected cells (Figure 2A), suggesting that Akt may induce growth arrest by upregulating p53 and p21. To determine the role of p21 in Akt-induced cell growth arrest, we infected primary cultured mouse embryonic fibroblasts (MEF) derived from *p21*-deficient or wild-type mice with AktCA. Similar to endothelial cells, the growth of wild-type MEF was markedly reduced by activation of Akt compared with mock infection (Figure 2B, $p21^{+/+}$). In contrast, Akt-induced cell growth arrest was restored in *p21*-deficient MEF (Figure 2B, $p21^{-/-}$), suggesting that p21 is essential for Akt-induced growth arrest of these cells. It has been reported that expression of p21 is regulated by p53-dependent or -independent transcriptional mechanisms (el-Deiry *et al*, 1993) as well as protein degradation (Maki and Howley, 1997). To investigate the mechanism by which Akt activation increases p21 expression, we assessed the stability of p21 protein and the extent of *p21* transcription. The half-life of p21 protein did not differ between mock- and AktCA-infected endothelial cells (Figure 2C). Northern blot analysis revealed that the level of *p21* mRNA was significantly increased in Akt-infected cells compared with mock-infected cells (Figure 2D). Activation of Akt enhanced transcription of the luciferase reporter gene controlled by the promoter fragment of the human *p21* gene (Figure 2E), indicating that activation of Akt caused the transcriptional upregulation of p21 expression.

Critical role of p53 transcriptional activity in Akt-induced growth arrest

To ascertain whether Akt activation induces the transcriptional activity of p53, we transfected Akt-infected endothelial

©2004 European Molecular Biology Organization

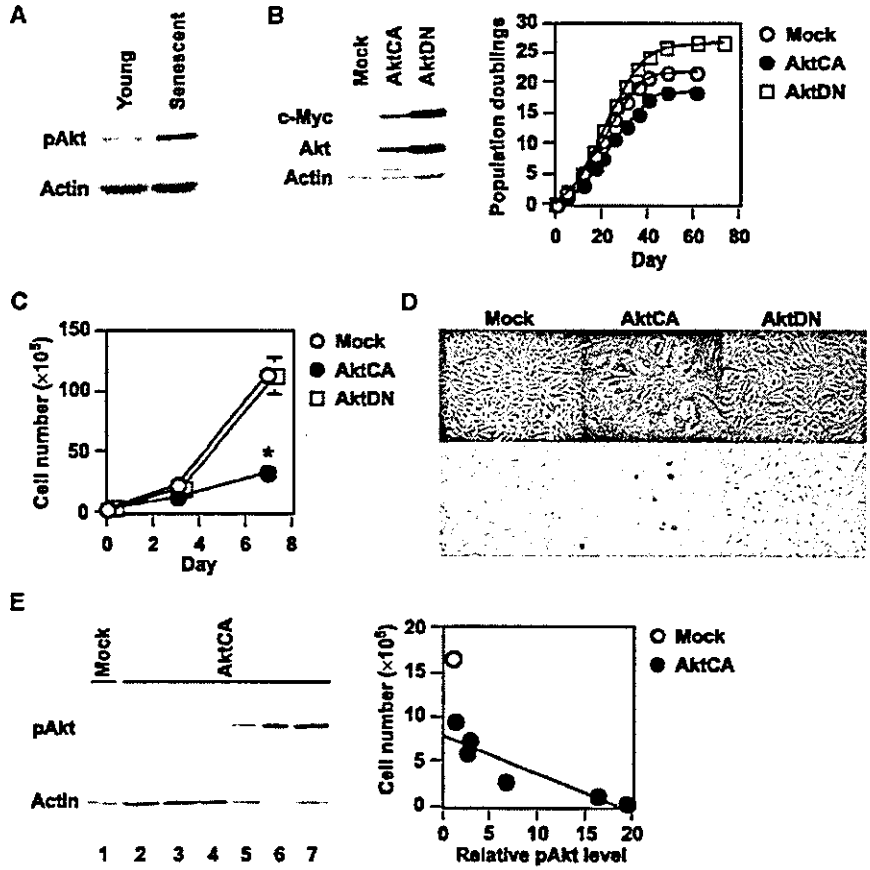

Figure 1 Akt negatively regulates the lifespan of primary cultured human endothelial cells. (**A**) Whole-cell lysates (30 μg) of young (passage 4) or senescent (passages 14–15) human endothelial cells were analyzed for the expression of phospho-Akt (pAkt, Ser473) and actin (loading control) by Western blotting. (**B**) Human endothelial cells were infected with pLNCX (Mock), AktCA or AktDN. After purification, infected cell populations were passaged until they underwent senescence, and the number of cumulative population doublings was determined. Similar results were obtained from three independent experiments. To validate the transduction of AktCA and AktDN, whole-cell lysates (30 μg) of each infected population were examined for the expression of exogenous myc-tagged Akt (c-Myc) and total Akt (Akt). (**C**) Human endothelial cells infected with pLNCX (Mock), AktCA or AktDN were purified with G418 for 7 days and seeded at a density of 3×10^5 cells per 100 mm plate on day 0. Cell number per 100 mm plate was then counted at indicated time points. $^*P<0.001$ versus Mock, ANOVA, $n=4$. (**D**) Cell morphology (upper panel) and senescence-associated β-galactosidase staining (lower panel) in endothelial cells infected with pLNCX (Mock), AktCA or AktDN. (**E**) Independent clones were isolated from pLNCX (Mock)- or AktCA-infected endothelial cells. At 30 days after isolation, the cell number of each clone was counted. Whole-cell lysates (~10 μg) of isolated clones were also prepared and analyzed for the expression of phospho-Akt by Western blotting (left panel, mock-infected clone for lane 1 and AktCA-infected clones for lanes 2–7). The cell number of each clone was as follows: 16.6×10^5 for lane 1; $6–10 \times 10^5$ for lanes 2–4; $0.1–2 \times 10^5$ for lanes 5–7. As the availability of samples was limited in the case of most AktCA-infected clones, the lysates used were less than 10 μg (lanes 5–7). Therefore, the levels of phospho-Akt were standardized on the basis of actin expression, and the relative level of phospho-Akt and the cell number of each clone were plotted in the graph (right panel, $r=0.92$, $P<0.01$). The corrected value of phospho-Akt in mock-infected clones (lane 1) is set at 1.

cells with the luciferase reporter gene containing 13 copies of the p53-binding consensus sequence (PG13). Introduction of AktCA induced *p53* promoter-driven luciferase activity compared with mock infection, but not luciferase activity driven by a promoter containing 15 copies of a similar sequence with mutation at critical positions (MG15) (Figure 3A). To further assess the relation between Akt and p53 transcription activity, we tested whether ablation of p53 could circumvent Akt-induced growth arrest. We infected human endothelial cells with a retroviral vector encoding the E6 oncoprotein of HPV16, which binds p53 and facilitates its destruction by ubiquitin-mediated proteolysis (pBabe E6). We also infected the same cells with the empty vector encoding resistance to puromycin alone (pBabe). Both cell populations were then subjected to infection with pLNCX or AktCA. Activation of Akt markedly inhibited the growth of pBabe-infected endothelial cells (Figure 3B, pBabe), while growth inhibition was completely abolished in E6-infected cells (Figure 3B, E6). Changes of cell morphology were also reversed to normal by introduction of E6 (Figure 3C). Ablation of p53 also lessened the decrease in the lifespan of AktCA-infected cells (Supplementary Figure 3). These results indicate a critical role of p53 in Akt-induced cell growth arrest. Introduction of AktCA did not induce p21 expression in E6-infected cells (Figure 3D), suggesting that constitutive activation of Akt increases induction of the transcription of *p21* by a p53-dependent mechanism and thereby promotes cell growth arrest.

©2004 European Molecular Biology Organization

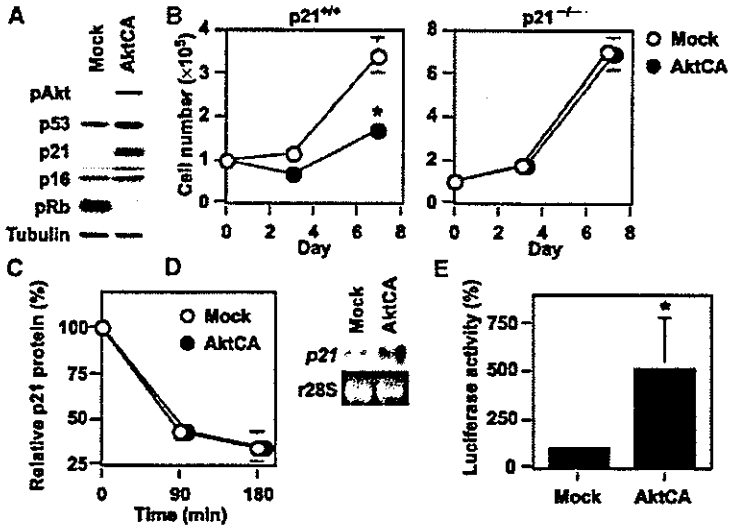

Figure 2 Upregulation of p21 is essential for Akt-induced growth arrest. (**A**) Whole-cell lysates (30 μg) of pLNCX (Mock)- or AktCA-infected endothelial cells on day 0 were examined for the expression of phospho-Akt (pAkt), cell cycle regulatory proteins and tubulin (loading control) by Western blotting. (**B**) MEF derived from wild-type ($p21^{+/+}$) or *p21*-deficient mice ($p21^{-/-}$) were infected with pLNCX (Mock) or AktCA, purified with G418 for 7 days and seeded at a density of 1×10^5 cells per 100 mm plate on day 0. Cell number per 100 mm plate was then counted at indicated time points. $^*P<0.001$ versus Mock, ANOVA, $n=4$. (**C**) Human endothelial cells infected with pLNCX (Mock) or AktCA were treated with cycloheximide (10 μg/ml) for the indicated time interval. Whole-cell lysates (30 μg) were then prepared at each time point and assayed for the expression of p21 and actin (loading control) by Western blotting. The graph indicates the results of densitometric analysis for the levels of p21 protein relative to actin expression. The value at time 0 is set at 100%. (**D**) Total RNA (30 μg) was extracted from human endothelial cells infected with pLNCX (Mock) or AktCA and analyzed for *p21* mRNA levels by Northern blotting (upper panel). Ribosomal RNA was used as an internal control (lower panel). (**E**) The luciferase reporter gene plasmid controlled by the promoter of the human *p21* gene was transfected into endothelial cells infected with pLNCX (Mock) or AktCA 24 h before the luciferase activity was measured. The activity in mock-infected cells is set at 100%. $^*P<0.05$ versus Mock, paired *t*-test, $n=4$.

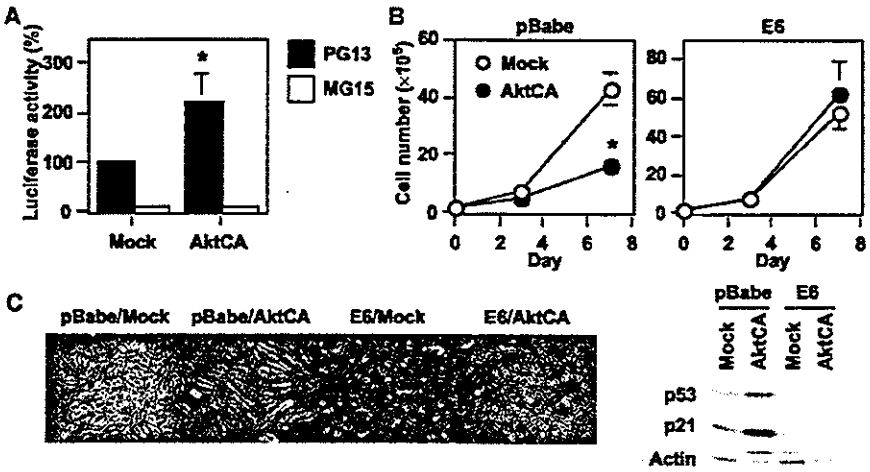

Figure 3 Critical role of p53 transcriptional activity in Akt-induced growth arrest. (**A**) The luciferase reporter gene plasmid pPG13-Luc containing the p53-binding sequence or pMG15-Luc containing the mutated p53-binding sequence was transfected into endothelial cells infected with pLNCX (Mock) or AktCA 24 h before the luciferase activity was measured. The activity of PG13-Luc in mock-infected cells is set at 100%. $^*P<0.005$ versus Mock, ANOVA, $n=4$. (**B**) Human endothelial cells were infected with pBabe (empty vector) or pBabe E6 and purified with puromycin. Infected cells were then transduced with pLNCX or AktCA as described in Figure 1C and seeded at a density of 2×10^5 cells per 100 mm plate on day 0. Cell number was then counted at indicated time points. $^*P<0.05$ versus Mock, ANOVA, $n=4$. (**C**) Morphology of cell populations prepared in (B). (**D**) Whole-cell lysates (30 μg) were extracted from cells prepared in (B) and examined for the expression of p53, p21 and actin (loading control).

Forkhead transcription factor mediates Akt-induced growth arrest

In *C. elegans*, a reduction-of-function mutation in the PI3K/Akt pathway leads to activation of the forkhead transcription factor DAF-16, resulting in extension of the lifespan, and this effect is inhibited by mutations of antioxidant genes (Murphy *et al*, 2003). Recent evidence indicates that the mammalian forkhead transcription factor FOXO3a (also known as FKHR-L1)

©2004 European Molecular Biology Organization

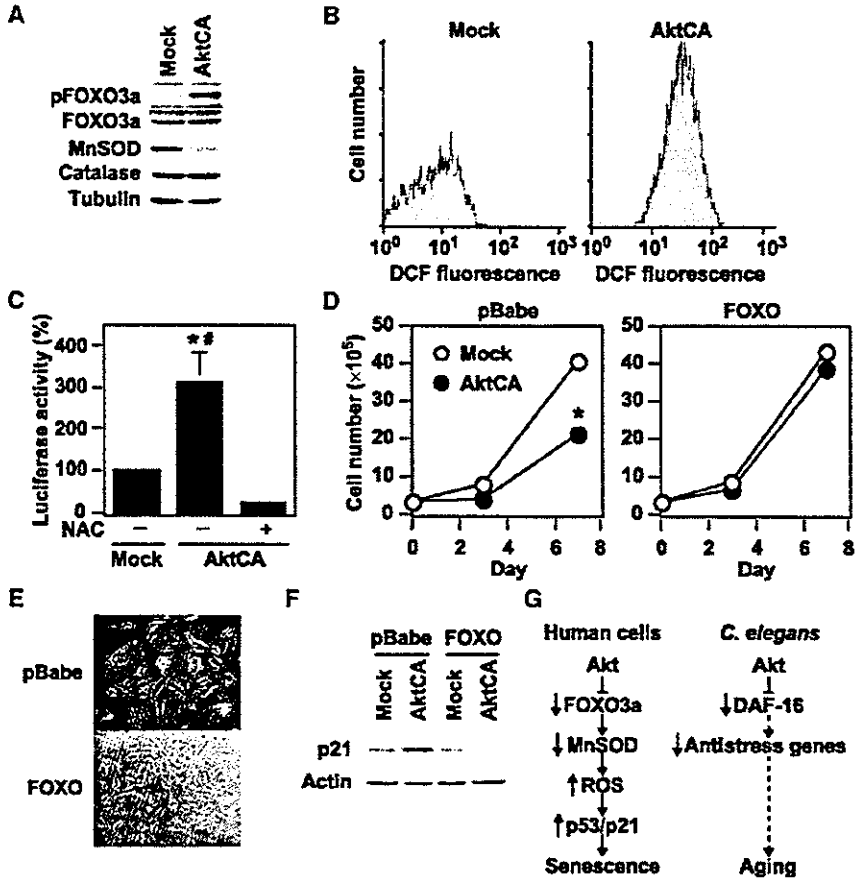

Figure 4 FOXO3a mediates Akt-induced growth arrest via the ROS/p53/p21-dependent mechanisms. (**A**) Whole-cell lysates (30 μg) of pLNCX (Mock)- or AktCA-infected endothelial cells were examined for expression of phospho-FOXO3a (pFOXO3a, Thr32), total FOXO3a (FOXO3a), MnSOD, catalase and tubulin (loading control) by Western blotting. (**B**) Human endothelial cells infected with pLNCX (Mock) or AktCA were loaded with DCF for 30 min and analyzed by FACS. Representative results from two independent experiments are shown. (**C**) The luciferase reporter gene plasmid PG13-Luc was transfected into endothelial cells infected with pLNCX (Mock) or AktCA and cultured in the absence or presence of NAC (0.5 mM). At 24 h after transfection, the luciferase activity was measured. The activity in mock-infected cells is set at 100%. $^{*}P<0.01$ versus Mock, $^{\#}P<0.001$ versus AktCA + NAC, ANOVA, $n=4$. (**D**) Human endothelial cells were infected with pBabe (empty vector) or pBabe mutant FOXO3a (FOXO). Infected cell populations were then transduced with pLNCX (Mock) or AktCA and seeded at a density of 3×10^5 cells per 100 mm plate on day 0. Cell number was then counted at indicated time points. $^{*}P<0.05$ versus Mock, ANOVA, $n=3$. (**E**) Morphology of Akt-infected cell populations prepared in (D). (**F**) Whole-cell lysates (30 μg) prepared in (D) were examined for the expression of p21 and actin (loading control) by Western blotting. Constitutive activation of Akt inhibits the transcriptional activity of FOXO3a and thereby downregulates *MnSOD*, leading to an increase of ROS that promotes senescence-like growth arrest via the p53/p21-dependent pathway. (**G**) Proposed signaling pathway of Akt-induced senescence in human endothelial cells compared with that in *C. elegans*. Akt inactivates FOXO3a and thereby downregulates its target antioxidant gene *MnSOD*, leading to an increase of ROS. ROS induces p53 activity, resulting in upregulation of p21 expression, which promotes cellular senescence in human endothelial cells. In *C. elegans*, the PI3K/Akt pathway also negatively regulates longevity by inactivating DAF-16 activity. This regulatory pathway partly involves the decreased expression of anti-stress genes including *SOD*.

upregulates radical scavenger genes that have a protective effect against oxidative damage in human cells (Kops *et al*, 2002; Nemoto and Finkel, 2002). To investigate the role of FOXO3a in Akt-induced growth arrest, we examined the expression of FOXO3a and antioxidant genes. Phosphorylated FOXO3a (the inactive form) was increased in AktCA-infected endothelial cells compared with mock-infected cells (Figure 4A). The level of manganese superoxide dismutase (MnSOD), but not catalase, was reduced in AktCA-infected endothelial cells (Figure 4A). Consistent with the decreased level of MnSOD, AktCA-infected endothelial cells exhibited an increase of reactive oxygen species (ROS), as assessed using the redox-sensitive fluorophore 2′,7′-dichlorofluorescein diacetate (DCF) (Figure 4B). Since oxidative stress is postulated to induce the activation of p53 (Finkel and Holbrook, 2000), we examined the effect of an ROS scavenger, *N*-acetyl cysteine (NAC), on *p53* promoter activity (PG13) in AktCA-infected endothelial cells. The enhancement of *p53* promoter-driven luciferase activity by AktCA was significantly lessened after treatment with NAC, suggesting that ROS are involved in Akt-induced senescence-like growth arrest (Figure 4C). To further determine the causal link between Akt-induced growth arrest and phosphorylation of FOXO3a, we tested a mutated FOXO3a that was resistant to phosphorylation by Akt. Introduction of this FOXO3a mutant prevented senescence-like growth arrest and cellular morphological changes induced by activation of

 ©2004 European Molecular Biology Organization

Akt (Figures 4D and E). Moreover, induction of p21 expression by Akt activation was effectively inhibited by the mutant form of FOXO3a (Figure 4F). These results suggest that constitutive activation of Akt inhibits the transcriptional activity of FOXO3a and thereby downregulates *MnSOD*, leading to an increase of ROS that promotes senescence-like growth arrest via the p53/p21-dependent pathway (Figure 4G). This signaling pathway could be recaptured in endothelial cells undergoing replicative senescence (Supplementary Figure 4), which suggests that Akt-induced growth arrest is relevant to physiological senescence and may also be involved in human vasculopathy.

Pathophysiological role of Akt-induced endothelial cell senescence

To investigate whether atherogenic stimuli could activate Akt in human atheroma tissues, we examined Akt activity in coronary arteries obtained at autopsy from patients who had ischemic heart disease. We detected Akt activity in endothelial cells on the surface of coronary atherosclerotic lesions, but not in those of the internal mammary arteries from the same patients, which showed minimal atherosclerotic changes (Figure 5A). To investigate the potential role of Akt-induced endothelial senescence in the pathogenesis of vasculopathy, we examined the effect of Akt on angiogenic activity and the expression of proinflammatory molecules. Tube formation by AktCA-infected endothelial cells was significantly reduced compared with that by mock-infected cells (Figure 5B). In addition, expression of intercellular adhesion molecule (ICAM)-1 was increased in AktCA-infected endothelial cells (Figure 5C). To further explore the role of Akt-induced senescence, we tested the influence of insulin on endothelial cell senescence. Treatment with insulin at a pathological dose caused increases in phospho-FOXO3a and p53 activity (Figures 6A and B), which were comparable to the changes seen in AktCA-infected cells. This increase was inhibited by introduction of AktDN (data not shown), indicating that it was dependent on Akt activity. Insulin induced p53 activity in a dose-dependent manner (Figure 6B). Moreover, continuous incubation with insulin was found to accelerate senescence of human endothelial cells, and this effect was also dose dependent (Figure 6C). Thus, it is conceivable that constitutive activation of Akt by growth factors may promote endothelial cell senescence and thereby contribute to vascular pathophysiology.

Discussion

Our results suggested a critical role of Akt activation in regulating the lifespan of primary cultured human cells in a manner similar to the control of longevity by the PI3K/Akt

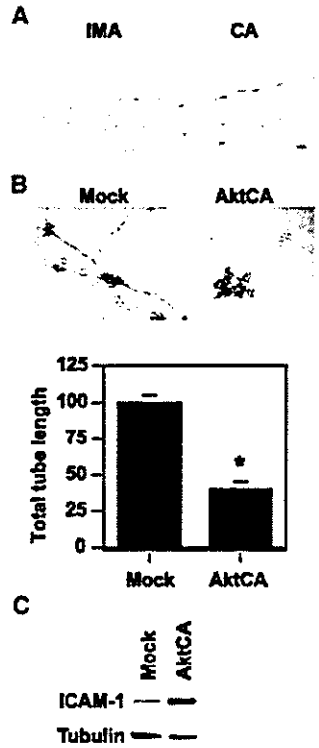

Figure 5 Pathophysiological role of Akt-induced endothelial cell senescence. (**A**) Immunohistochemistry for phospho-Akt (brown) in the coronary arteries (CA) and the internal mammary arteries (IMA) from the same patients. Scale bar: 10 μm. (**B**) Tube formation assay. Human endothelial cells infected with pLNCX (Mock) or AktCA were seeded onto Matrigel. After 48 h, the total tube length was estimated by an angiogenesis image analyzer (Kurabo, Osaka, Japan). The graph shows relative tube length in Mock- and AktCA-infected cells. The length in Mock-infected cells is set at 100%. $^{*}P<0.005$ versus Mock, unpaired *t*-test, $n=4$. (**C**) Whole-cell lysates (30 μg) of pLNCX (Mock)- or AktCA-infected endothelial cells were examined for the expression of ICAM-1 and tubulin (loading control) by Western blotting.

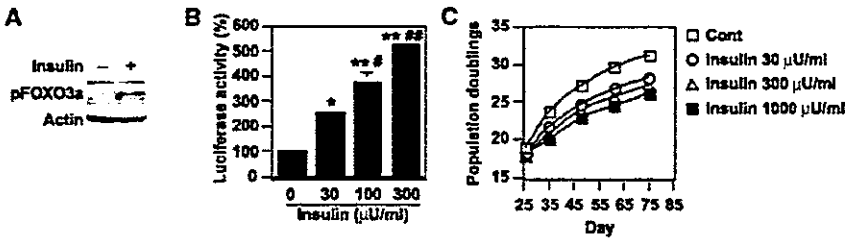

Figure 6 Insulin promotes endothelial cell senescence. (**A**) Whole-cell lysates (30 μg) of human endothelial cells treated with insulin (1000 μU/ml) for 30 min were analyzed for the levels of phosphorylated FOXO3a and actin (loading control) by Western blotting. (**B**) The luciferase reporter gene plasmid PG13-Luc was transfected into endothelial cells in the presence of insulin at the indicated dose. At 24 h after transfection, the luciferase activity was measured. The activity in controls is set at 100%. $^{*}P<0.05$, $^{**}P<0.0001$ versus control, $^{\#}P<0.01$, $^{\#\#}P<0.001$ versus insulin 30 μU/ml, $n=4$. (**C**) Human endothelial cells were cultured in the presence of insulin at the indicated dose and passaged. The number of cumulative population doublings was determined ($n=3$).

©2004 European Molecular Biology Organization

signaling pathway in *C. elegans*. We have previously demonstrated that senescent endothelial cells are present in human atherosclerotic plaques, but not nonatherosclerotic lesions, and express high levels of proinflammatory molecules that are known to promote atherogenesis (Minamino *et al*, 2002). Since Akt is known to be activated by various atherogenic stimuli (Cantley, 2002), our findings imply that constitutive activation of Akt by atherogenic stimuli may induce endothelial cell senescence in atheroma tissue and thereby contribute to atherogenesis. Consistent with this hypothesis, we observed that Akt was phosphorylated in human atheroma but not in normal arteries, and that expression of proinflammatory molecules was increased in AktCA-infected endothelial cells compared with mock-infected cells. Moreover, insulin increased p53 activity via an Akt-dependent mechanism and reduced the lifespan of endothelial cells. Thus, an Akt-induced senescence-like phenotype may be particularly involved in diabetic vasculopathy, since hyperinsulinemia could constitutively activate Akt in endothelial cells.

Although one supposes that Akt-induced senescence might be an artifact, the following points suggest that our findings are valid. First, we observed that Akt activity was increased in endothelial cells undergoing replicative senescence and that inhibition of this endogenous increase in Akt activity by AktDN led to prolongation of the cellular lifespan. This is compatible with many earlier studies demonstrating that reduction-of-function mutations in the insulin/PI3K/Akt pathway extend longevity in organisms ranging from yeast to mice (Longo and Finch, 2003). This signaling pathway (including phosphorylation of FOXO3a and downregulation of MnSOD induced by Akt) could be recaptured in endothelial cells undergoing replicative senescence (Supplementary Figure 4), which suggests that Akt-induced growth arrest may be relevant to physiological senescence. Second, we found that growth was significantly decreased in cloned populations obtained from cells infected with AktCA that exhibited a moderate increase in Akt activity (Figure 1, lanes 2–4). The level of Akt activity in these cells was similar to that in endothelial cells undergoing replicative senescence, suggesting that a physiological level of Akt activation may be able to promote cellular senescence. Third, we found that phospho-FOXO3a levels in AktCA-infected cells were comparable to those in endothelial cells stimulated by insulin at the level seen in patients with type II diabetes. The p53 transcriptional activity in AktCA-infected cells was also similar to that of cells treated with insulin. These results indicate that the pathophysiological activation of Akt was mimicked by infection with AktCA.

Gain-of-function mutations in the PI3K/Akt signaling pathway are frequently found in human cancers (Testa and Bellacosa, 2001). Thus, Akt-induced growth arrest may be another antitumorigenesis mechanism similar to Ras-induced senescence (Serrano *et al*, 1997; Campisi, 2001; Wright and Shay, 2001). We found that ablation of p53 prevented Akt-induced growth arrest, whereas both the p53- and p16-dependent pathways are reported to be essential for Ras-induced senescence (Serrano *et al*, 1997; Lin *et al*, 1998). Oncogenic Ras also induced premature senescence of primary cultured human vascular cells, which was suppressed by inhibition of mitogen-activated protein kinase kinase but not PI3K (Minamino *et al*, 2003), suggesting that Akt-induced growth arrest may be distinct from Ras-induced senescence. A recent study demonstrated that senescent cells could potentiate the oncogenic transformation of nearby normal cells (Krtolica *et al*, 2001), which suggests that induction of senescence by Akt as well as Ras may actually be pro-oncogenic.

We found that Akt increased the transcriptional activity of p53, resulting in upregulation of *p21* in primary cultured human endothelial cells. Our results are consistent with previous reports that Akt mediates induction of p21 expression by various stimuli in myoblasts and vascular cells (Lawlor and Rotwein, 2000a, b; Schonherr *et al*, 2001). However, Akt is also reported to induce cytoplasmic localization of p21 (Zhou *et al*, 2001a), thereby promoting cell proliferation, and to promote nuclear translocation of Mdm2 (a negative regulator of p53), leading to a reduction of both p53 levels and transactivation (Mayo and Donner, 2001; Zhou *et al*, 2001b). Such changes were not observed in human endothelial cells (H Miyauchi, unpublished data). It is noteworthy that most other studies have examined immortal cells, in which the normal cell cycle machinery might be impaired, and the effects of constitutive Akt activation have not been explored. Although the effects of tissue-specific transgenic expression of constitutively activated *Akt* alleles have been reported in several different murine models, most of these animals do not develop tumors (Vivanco and Sawyers, 2002), suggesting that activation of Akt is insufficient to cause cancer unless combined with other oncogenic stimuli. Thus, like Ras, Akt may promote cell proliferation and survival or senescence-like growth arrest, depending on various factors including the cellular context as well as the duration and extent of its activation.

In conclusion, we found that Akt negatively regulates the lifespan of primary cultured human endothelial cells via the p53/p21-dependent pathway, and this action is mediated at least partly by the forkhead transcription factor that regulates cellular ROS levels. Our data not only support the previous findings about the signaling pathway for longevity in *C. elegans*, but also provide a novel insight for research on the treatments of human vasculopathy and cancer.

Materials and methods

Cell culture

Human aortic endothelial cells, human dermal microvascular endothelial cells and human umbilical vein endothelial cells were purchased from Bio Whittaker (Walkersville, MD), and cultured according to the manufacturer's instructions. These cells gave similar results (data not shown). We defined senescent cells as the cultures that do not increase in the cell number and remain subconfluent for 2 weeks. We confirmed the senescent phenotype with SA-β-gal activity assay. Wild-type and *p21*-deficient MEFs were prepared from day 13.5 embryos derived from crosses between $p21^{+/-}$ mice (Jackson, Bar Harbor, ME) and cultured in DMEM plus 10% fetal bovine serum. Senescence-associated β-galactosidase staining was performed as described (Minamino *et al*, 2002). Tube formation assay was performed according to the manufacturer's instructions (BioCoat Angiogenesis System, Clontech, Palo Alto, CA).

Retroviral infection

The following plasmids were used for generating retroviruses: pLNCX (Clontech, Palo Alto, CA) and pBabe (a gift from Dr CW Lowe, Cold Spring Harbor Laboratory, Cold Spring Harbor, NY). We created the pLNCX-based vector expressing a constitutively active form of Akt (AktCA) or a dominant-negative form of Akt (AktDN) by using the fragment derived from the plasmid pBS-CA-Akt or

©2004 European Molecular Biology Organization

pBS-DN-Akt (Fujishiro *et al*, 2001), respectively (a gift from Dr T Asano, Tokyo University, Tokyo, Japan). The pBabe-based vector expressing a mutant form of FOXO3a was constructed by using the fragment derived from pECE FOXO3aTM (Brunet *et al*, 1999) (a gift from Dr ME Greenberg, Harvard Medical School, Boston, MA). We also constructed the pBabe-based vector expressing E6 (pBabe E6). Details of the construct are available upon request. Retroviral stocks were generated by transient transfection of packaging cell line (PT67, Clontech) and stored at −80°C until use. Human endothelial cells (passage 4–6) were plated at 5×10^5 cells per 100-mm-diameter dish 24 h before infections. For infections, the culture medium was replaced by retroviral stocks supplemented with 8 μg/ml polybrene (Sigma, Tokyo, Japan). At 48 h after infections, the infected cell populations were selected by culture in 500 μg/ml G418 for 7 days (pLNCX-based vectors). After selection, $1–3 \times 10^5$ cells were seeded onto 100-mm-diameter dishes on the 8th day postinfection. The 8th day after infection is designated as day 0. For double infection, endothelial cells were infected with pBabe, pBabe FOXO3a or pBabe E6 purified with 0.8 μg/ml puromycin for 4 days and subjected to the second infection as described above.

Western blotting and antibodies

Whole-cell lysates (30 μg) were resolved by SDS polyacrylamide gel electrophoresis (PAGE). Proteins were transferred onto a polyvinylidene difluoride (PVDF) membrane (Millipore, Bedford, MA) and incubated with the first antibody followed by an anti-rabbit immunoglobulin G–horseradish peroxidase antibody or anti-mouse immunoglobulin G–horseradish peroxidase antibody (Jackson, West Grove, PA). Specific proteins were detected using enhanced chemiluminescence (Amersham, Tokyo, Japan). The first antibodies used for Western blotting are as follows: antibodies to Akt, p53, ICAM-1, actin and tubulin (Santa Cruz, Santa Cruz, CA); antibodies to retinoblastoma protein and p16 (Pharmingen, Tokyo, Japan); anti-p21 antibody (Oncogene, Cambridge, MA); anti-phospho-Akt (Ser473) antibody (Cell Signaling, Beverly, MA); anti-catalase antibody (Sigma); antibodies to FOXO3a, phospho-FOXO3a (Thr32) and MnSOD (Upstate Biotechnology, Lake Placid, NY).

Northern blotting

Total RNA (30 μg) was extracted using RNA zol B (Tel Test, Friendswood, TX) according to the manufacturer's instructions, separated on a formaldehyde denaturing gel and transferred to a nylon membrane (Amersham). The blot was then hybridized with radiolabeled p21 cDNA probes using the Quickhyb hybridization solution (Stratagene, Tokyo, Japan) according to the manufacturer's instructions.

Luciferase assays

The reporter gene plasmid (1 μg) was transfected into endothelial cells infected with pLNCX (Mock) or AktCA 24 h before luciferase assay. The control vector encoding *Renilla* luciferase (0.1 μg) was co-transfected for an internal control. Luciferase assay was carried out using a dual-luciferase reporter assay system (Promega, Madison, WI) according to the manufacturer's instructions. The plasmids pPG13-Luc, pPG15-Luc and pWWP-LUC-1 (el-Deiry *et al*, 1993) were a gift from Dr B Vogelstein (Johns Hopkins University, Baltimore, MD).

Tissue specimens and histology

Human coronary arteries and internal mammary arteries were obtained from four autopsied individuals who had ischemic heart disease. For immunohistochemistry, the frozen sections (6 μm) were treated with 0.3% hydrogen peroxide in methanol for 20 min, preincubated with 5% goat serum and then treated with anti-phospho-Akt antibody (1:100; Santa Cruz, Santa Cruz, CA) for 1 h at 37°C. Next, the sections were incubated with a biotinylated goat secondary antibody, treated with the avidin-biotin complex (Elite ABC kit, Vector, Burlingame, CA) and stained with diaminobenzidine tetrahydrochloride and hydrogen peroxide. To verify the specificity of the first antibodies, we performed a control staining with nonimmune IgG and excluded the possibility of nonspecific signals. The studies on human samples were approved by our institutional review board.

Statistical analysis

All values were expressed as mean ± s.e.m. Comparison of results between different groups was performed by one-way analysis of variance, paired *t*-test and unpaired *t*-test using StatView 4.5 (Abacus Concepts, Berkeley, CA).

Supplementary data

Supplementary data are available at *The EMBO Journal* Online.

Acknowledgements

We thank Dr B Vogelstein, SW Lowe, ME Greenberg and T Asano for reagents. This work was supported by grants from Takeda Medical Research Foundation, Takeda Science Foundation, Japan Heart Foundation, Mochida Memorial Foundation, Uehara Memorial Foundation, Mitsubishi Pharma Research Foundation and the Ministry of Education, Science, Sports, and Culture of Japan (to TM and IK).

Competing interests statement

The authors declare that they have no competing financial interests.

References

Bluher M, Kahn BB, Kahn CR (2003) Extended longevity in mice lacking the insulin receptor in adipose tissue. *Science* **299:** 572–574

Blume-Jensen P, Hunter T (2001) Oncogenic kinase signalling. *Nature* **411:** 355–365

Brunet A, Bonni A, Zigmond MJ, Lin MZ, Juo P, Hu LS, Anderson MJ, Arden KC, Blenis J, Greenberg ME (1999) Akt promotes cell survival by phosphorylating and inhibiting a Forkhead transcription factor. *Cell* **96:** 857–868

Campisi J (2001) Cellular senescence as a tumor-suppressor mechanism. *Trends Cell Biol* **11:** S27–S31

Cantley LC (2002) The phosphoinositide 3-kinase pathway. *Science* **296:** 1655–1657

Cardone MH, Roy N, Stennicke HR, Salvesen GS, Franke TF, Stanbridge E, Frisch S, Reed JC (1998) Regulation of cell death protease caspase-9 by phosphorylation. *Science* **282:** 1318–1321

Cheng JQ, Altomare DA, Klein MA, Lee WC, Kruh GD, Lissy NA, Testa JR (1997) Transforming activity and mitosis-related expression of the AKT2 oncogene: evidence suggesting a link between cell cycle regulation and oncogenesis. *Oncogene* **14:** 2793–2801

Cheng JQ, Ruggeri B, Klein WM, Sonoda G, Altomare DA, Watson DK, Testa JR (1996) Amplification of AKT2 in human pancreatic cells and inhibition of AKT2 expression and tumorigenicity by antisense RNA. *Proc Natl Acad Sci USA* **93:** 3636–3641

Cristofalo VJ, Allen RG, Pignolo RJ, Martin BG, Beck JC (1998) Relationship between donor age and the replicative lifespan of human cells in culture: a reevaluation. *Proc Natl Acad Sci USA* **95:** 10614–10619

Datta SR, Brunet A, Greenberg ME (1999) Cellular survival: a play in three Akts. *Genes Dev* **13:** 2905–2927

Datta SR, Dudek H, Tao X, Masters S, Fu H, Gotoh Y, Greenberg ME (1997) Akt phosphorylation of BAD couples survival signals to the cell-intrinsic death machinery. *Cell* **91:** 231–241

del Peso L, Gonzalez-Garcia M, Page C, Herrera R, Nunez G (1997) Interleukin-3-induced phosphorylation of BAD through the protein kinase Akt. *Science* **278:** 687–689

Diehl JA, Cheng M, Roussel MF, Sherr CJ (1998) Glycogen synthase kinase-3beta regulates cyclin D1 proteolysis and subcellular localization. *Genes Dev* **12:** 3499–3511

el-Deiry WS, Tokino T, Velculescu VE, Levy DB, Parsons R, Trent JM, Lin D, Mercer WE, Kinzler KW, Vogelstein B (1993) WAF1, a potential mediator of p53 tumor suppression. *Cell* **75:** 817–825

Fabrizio P, Liou LL, Moy VN, Diaspro A, SelverstoneValentine J, Gralla EB, Longo VD (2003) SOD2 functions downstream of Sch9 to extend longevity in yeast. *Genetics* **163:** 35–46

Fabrizio P, Pozza F, Pletcher SD, Gendron CM, Longo VD (2001) Regulation of longevity and stress resistance by Sch9 in yeast. *Science* **292:** 288–290

©2004 European Molecular Biology Organization

Faragher RG, Kipling D (1998) How might replicative senescence contribute to human ageing? *BioEssays* **20:** 985–991
Finkel T, Holbrook NJ (2000) Oxidants, oxidative stress and the biology of ageing. *Nature* **408:** 239–247
Fujishiro M, Gotoh Y, Katagiri H, Sakoda H, Ogihara T, Anai M, Onishi Y, Ono H, Funaki M, Inukai K, Fukushima Y, Kikuchi M, Oka Y, Asano T (2001) MKK6/3 and p38 MAPK pathway activation is not necessary for insulin-induced glucose uptake but regulates glucose transporter expression. *J Biol Chem* **276:** 19800–19806
Guarente L, Kenyon C (2000) Genetic pathways that regulate ageing in model organisms. *Nature* **408:** 255–262
Hayflick L (1975) Current theories of biological aging. *Fed Proc* **34:** 9–13
Holzenberger M, Dupont J, Ducos B, Leneuve P, Geloen A, Even PC, Cervera P, Le Bouc Y (2003) IGF-1 receptor regulates lifespan and resistance to oxidative stress in mice. *Nature* **421:** 182–187
Honda Y, Honda S (1999) The daf-2 gene network for longevity regulates oxidative stress resistance and Mn-superoxide dismutase gene expression in *Caenorhabditis elegans*. *FASEB J* **13:** 1385–1393
Kenyon C (2001) A conserved regulatory system for aging. *Cell* **105:** 165–168
Kenyon C, Chang J, Gensch E, Rudner A, Tabtiang R (1993) A *C. elegans* mutant that lives twice as long as wild type. *Nature* **366:** 461–464
Kops GJ, Dansen TB, Polderman PE, Saarloos I, Wirtz KW, Coffer PJ, Huang TT, Bos JL, Medema RH, Burgering BM (2002) Forkhead transcription factor FOXO3a protects quiescent cells from oxidative stress. *Nature* **419:** 316–321
Krtolica A, Parrinello S, Lockett S, Desprez PY, Campisi J (2001) Senescent fibroblasts promote epithelial cell growth and tumorigenesis: a link between cancer and aging. *Proc Natl Acad Sci USA* **98:** 12072–12077
Lawlor MA, Rotwein P (2000a) Coordinate control of muscle cell survival by distinct insulin-like growth factor activated signaling pathways. *J Cell Biol* **151:** 1131–1140
Lawlor MA, Rotwein P (2000b) Insulin-like growth factor-mediated muscle cell survival: central roles for Akt and cyclin-dependent kinase inhibitor p21. *Mol Cell Biol* **20:** 8983–8995
Lee RY, Hench J, Ruvkun G (2001) Regulation of *C. elegans* DAF-16 and its human ortholog FKHRL1 by the daf-2 insulin-like signaling pathway. *Curr Biol* **11:** 1950–1957
Lin AW, Barradas M, Stone JC, van Aelst L, Serrano M, Lowe SW (1998) Premature senescence involving p53 and p16 is activated in response to constitutive MEK/MAPK mitogenic signaling. *Genes Dev* **12:** 3008–3019
Lin K, Dorman JB, Rodan A, Kenyon C (1997) daf-16: An HNF-3/forkhead family member that can function to double the life-span of *Caenorhabditis elegans*. *Science* **278:** 1319–1322
Lin K, Hsin H, Libina N, Kenyon C (2001) Regulation of the *Caenorhabditis elegans* longevity protein DAF-16 by insulin/IGF-1 and germline signaling. *Nat Genet* **28:** 139–145
Longo VD, Finch CE (2003) Evolutionary medicine: from dwarf model systems to healthy centenarians? *Science* **299:** 1342–1346
Maki CG, Howley PM (1997) Ubiquitination of p53 and p21 is differentially affected by ionizing and UV radiation. *Mol Cell Biol* **17:** 355–363
Mayo LD, Donner DB (2001) A phosphatidylinositol 3-kinase/Akt pathway promotes translocation of Mdm2 from the cytoplasm to the nucleus. *Proc Natl Acad Sci USA* **98:** 11598–11603
Medema RH, Kops GJ, Bos JL, Burgering BM (2000) AFX-like Forkhead transcription factors mediate cell-cycle regulation by Ras and PKB through p27kip1. *Nature* **404:** 782–787
Minamino T, Miyauchi H, Yoshida T, Ishida Y, Yoshida H, Komuro I (2002) Endothelial cell senescence in human atherosclerosis: role of telomere in endothelial dysfunction. *Circulation* **105:** 1541–1544
Minamino T, Yoshida T, Tateno K, Miyauchi H, Zou Y, Toko H, Komuro I (2003) Ras-induced vascular smooth muscle cell senescence in human atherosclerosis. *Circulation* **108:** 2264–2269
Morris JZ, Tissenbaum HA, Ruvkun G (1996) A phosphatidylinositol-3-OH kinase family member regulating longevity and diapause in *Caenorhabditis elegans*. *Nature* **382:** 536–539
Murphy CT, McCarroll SA, Bargmann CI, Fraser A, Kamath RS, Ahringer J, Li H, Kenyon C (2003) Genes that act downstream of DAF-16 to influence the lifespan of *Caenorhabditis elegans*. *Nature* **424:** 277–283
Nemoto S, Finkel T (2002) Redox regulation of forkhead proteins through a p66shc-dependent signaling pathway. *Science* **295:** 2450–2452
Ogg S, Paradis S, Gottlieb S, Patterson GI, Lee L, Tissenbaum HA, Ruvkun G (1997) The Fork head transcription factor DAF-16 transduces insulin-like metabolic and longevity signals in *C. elegans*. *Nature* **389:** 994–999
Paradis S, Ruvkun G (1998) *Caenorhabditis elegans* Akt/PKB transduces insulin receptor-like signals from AGE-1 PI3 kinase to the DAF-16 transcription factor. *Genes Dev* **12:** 2488–2498
Rohme D (1981) Evidence for a relationship between longevity of mammalian species and life spans of normal fibroblasts *in vitro* and erythrocytes *in vivo*. *Proc Natl Acad Sci USA* **78:** 5009–5013
Schonherr E, Levkau B, Schaefer L, Kresse H, Walsh K (2001) Decorin-mediated signal transduction in endothelial cells. Involvement of Akt/protein kinase B in up-regulation of p21(WAF1/CIP1) but not p27(KIP1). *J Biol Chem* **276:** 40687–40692
Serrano M, Lin AW, McCurrach ME, Beach D, Lowe SW (1997) Oncogenic ras provokes premature cell senescence associated with accumulation of p53 and p16INK4a. *Cell* **88:** 593–602
Shin I, Yakes FM, Rojo F, Shin NY, Bakin AV, Baselga J, Arteaga CL (2002) PKB/Akt mediates cell-cycle progression by phosphorylation of p27(Kip1) at threonine 157 and modulation of its cellular localization. *Nat Med* **8:** 1145–1152
Tatar M, Kopelman A, Epstein D, Tu MP, Yin CM, Garofalo RS (2001) A mutant *Drosophila* insulin receptor homolog that extends life-span and impairs neuroendocrine function. *Science* **292:** 107–110
Testa JR, Bellacosa A (2001) AKT plays a central role in tumorigenesis. *Proc Natl Acad Sci USA* **98:** 10983–10985
Thompson KV, Holliday R (1983) Genetic effects on the longevity of cultured human fibroblasts. II. DNA repair deficient syndromes. *Gerontology* **29:** 83–88
Viglietto G, Motti ML, Bruni P, Melillo RM, D'Alessio A, Califano D, Vinci F, Chiappetta G, Tsichlis P, Bellacosa A, Fusco A, Santoro M (2002) Cytoplasmic relocalization and inhibition of the cyclin-dependent kinase inhibitor p27(Kip1) by PKB/Akt-mediated phosphorylation in breast cancer. *Nat Med* **8:** 1136–1144
Vivanco I, Sawyers CL (2002) The phosphatidylinositol 3-Kinase AKT pathway in human cancer. *Nat Rev Cancer* **2:** 489–501
Weinstein BS, Ciszek D (2002) The reserve-capacity hypothesis: evolutionary origins and modern implications of the trade-off between tumor-suppression and tissue-repair. *Exp Gerontol* **37:** 615–627
Wright WE, Shay JW (2001) Cellular senescence as a tumor-protection mechanism: the essential role of counting. *Curr Opin Genet Dev* **11:** 98–103
Zhou BP, Liao Y, Xia W, Spohn B, Lee MH, Hung MC (2001a) Cytoplasmic localization of p21Cip1/WAF1 by Akt-induced phosphorylation in HER-2/neu-overexpressing cells. *Nat Cell Biol* **3:** 245–252
Zhou BP, Liao Y, Xia W, Zou Y, Spohn B, Hung MC (2001b) HER-2/neu induces p53 ubiquitination via Akt-mediated MDM2 phosphorylation. *Nat Cell Biol* **3:** 973–982

©2004 European Molecular Biology Organization

Available online at www.sciencedirect.com
SCIENCE DIRECT®
Biochemical and Biophysical Research Communications 314 (2004) 849–853
BBRC
www.elsevier.com/locate/ybbrc

Role of Na^+–Ca^{2+} exchanger in myocardial ischemia/reperfusion injury: evaluation using a heterozygous Na^+–Ca^{2+} exchanger knockout mouse model

Masashi Ohtsuka,[a] Hiroyuki Takano,[a] Masashi Suzuki,[b] Yunzeng Zou,[a] Hiroshi Akazawa,[a] Masaji Tamagawa,[b] Koji Wakimoto,[c] Haruaki Nakaya,[b] and Issei Komuro[a,*]

[a] *Department of Cardiovascular Science and Medicine, Chiba University Graduate School of Medicine, 1-8-1 Inohana, Chuo-ku, Chiba 260-8670, Japan*
[b] *Department of Pharmacology, Chiba University Graduate School of Medicine, 1-8-1 Inohana, Chuo-ku, Chiba 260-8670, Japan*
[c] *Discovery Research Laboratory, Tanabe Seiyaku Co. Ltd., 3-16-89 Kashima, Yodogawa-ku, Osaka 532-8505, Japan*

Received 5 December 2003

Abstract

We used Na^+–Ca^{2+} exchanger (NCX) knockout mice to evaluate the effects of NCX in cardiac function and the infarct size after ischemia/reperfusion injury. The contractile function in NCX KO mice hearts was significantly better than that in wild type (WT) mice hearts after ischemia/reperfusion and the infarct size was significantly small in NCX KO mice hearts compared with that in WT mice hearts. NCX is critically involved in the development of ischemia/reperfusion-induced myocardial injury and therefore the inhibition of NCX function may contribute to cardioprotection against ischemia/reperfusion injury.
© 2003 Elsevier Inc. All rights reserved.

Keywords: Sodium–calcium exchanger; Knockout mouse; Heart; Ischemia/reperfusion injury

The Na^+–Ca^{2+} exchanger (NCX) is an important electrogenic transporter in maintaining calcium homeostasis in a variety of mammalian organs [1]. NCX catalyzes electrogenic exchange of Na^+ and Ca^{2+} across the plasma membrane in either the Ca^{2+}-efflux (the forward mode) or Ca^{2+}-influx (the reverse mode), depending on the electrochemical gradients of the substrate ions. In the heart, NCX plays an important role in excitation–contraction coupling as the dominant myocardial Ca^{2+}-efflux system [2]. On the other hand, the reverse mode of NCX is associated with in cytoplasmic Ca^{2+} levels in cardiomyocytes during digitalis treatment or ischemia/reperfusion [3]. It has been reported that NCX inhibitors and NCX antisense oligonucleotides protect the heart from ischemia/reperfusion injury [4,5]. However, two putative NCX inhibitors, KB-R7943 and SEA0400, have been reported to be not specific for NCX [6]. Therefore, it remains unclear whether NCX indeed plays a crucial role in mediating Ca^{2+} influx that leads to Ca^{2+} overload and cellular injury after myocardial ischemia, reperfusion injury. Using heterozygous NCX KO mice, we examined the role of NCX in myocardial ischemia/reperfusion injury.

Materials and methods

NCX KO mice. NCX knockout (KO) mice were generated as described previously [7]. Male heterozygous KO mice and wild type (WT) littermates 12 weeks old were used. All animal experiments were performed according to the *Guide for the Care and Use of Laboratory Animals* (NIH Publication No. 85-23, revised 1996).

Electrophysiology. Ventricular cells were prepared from adult mice hearts by standard enzymatic digestion [8]. Whole-cell membrane currents were recorded by the patch-clamp method and the current–voltage relationship was obtained by voltage clamp ramp pulses as described previously [9]. Under these conditions, the Ni^{2+}-sensitive current represents NCX current [10]. All data were acquired and analyzed by the pCLAMP (version 5.5; Axon Instrument) software.

Western blot analysis. Expression levels of dihydropyridine (DHP) receptor (L-type Ca^{2+} channel) and SR Ca^{2+}-ATPase 2 (SERCA2)

* Corresponding author. Fax: +81-43-226-2557.
E-mail address: komuro-tky@umin.ac.jp (I. Komuro).

0006-291X/$ - see front matter © 2003 Elsevier Inc. All rights reserved.
doi:10.1016/j.bbrc.2003.12.165

were analyzed by Western blot as described previously [11]. Briefly, tissue was homogenized in lysis buffer containing 25 mM Tris–HCl (pH 7.4), 25 mM NaCl, 0.5 mM EGTA, 10 mM sodium pyrophosphate, 1 mM sodium orthovanadate, 10 mM NaF, 10 nM okadaic acid, 1 mM PMSF, 20 μg/ml aprotinin, and 20 μg/ml leupeptin. Protein concentration was determined using a protein assay kit (Bio-Rad) and equal amounts of total protein (40 μg/lane) were separated on 8% SDS–polyacrylamide gel. Separated proteins were transferred to nitrocellulose membrane (Amersham Life Science). Membranes were incubated with anti-mouse dihydropyridine L-type Ca^{2+} channel α-2 subunit monoclonal antibody (Affinity Bioreagents) or anti-mouse SERCA2 monoclonal antibody (Affinity Bioreagents) at 4 °C overnight. After washing, the membranes were incubated with horseradish peroxidase-conjugated goat anti-mouse antibody for 1 h. Immunoreactive protein was visualized using an enhanced chemiluminescence detection kit (ECL, Amersham).

Ischemia/reperfusion. Hearts were excised from mice and connected to the perfusion cannula via the aorta as described previously [8]. Retrograde perfusion was maintained with Krebs–Henseleit solution. To evaluate the contractile function, a polyethylene film balloon was inserted into the cavity of the left ventricle through the left atrium. The balloon was filled with saline to adjust the baseline end-diastolic pressure to 5–10 mmHg. Hearts were subjected to no-flow, global ischemia by clamping the perfusion line. After 30 min of ischemia, the clamp was released and the hearts were reperfused for 120 min. Left ventricular developed pressure (LVDP) was designated as difference between systolic and diastolic pressures of the left ventricle. After 120 min, the heart was incubated for 5 min at 37 °C in a 1% solution of triphenyltetrazolium chloride (TTC). The sizes of infarcted area (pale) and viable ischemic–reperfused area (red) were measured by computed planimetry (Scion Image 1.62). Infarct size was calculated as described previously [12].

Statistics analysis. All data are presented as means ± SEM. Statistical analyses of the data were performed using Student's *t* test. Probability values less than 0.05 were considered to be significant.

Results

NCX current density and Western blot analysis

We previously reported that the protein content of NCX in NCX KO mice hearts was ~50% of that in WT mice hearts [13]. To elucidate the functional activity, we examined NCX current densities from −40 to 40 mV in WT ($n = 9$) and NCX KO ventricular cells ($n = 6$) (Fig. 1). The densities of the reverse mode of NCX at 40 mV in ventricular cells of KO mice (0.57 ± 0.07 pA/pF) were approximately half (55.4%) compared with those of WT mice (1.04 ± 0.14 pA/pF). These results suggest that the functional activity as well as the protein content of NCX in the myocardium of NCX KO mice is approximately half of those of WT mice.

Western blot analysis revealed that there was no difference in the protein levels of L-type Ca^{2+} channel and SERCA2 between the two groups (data not shown).

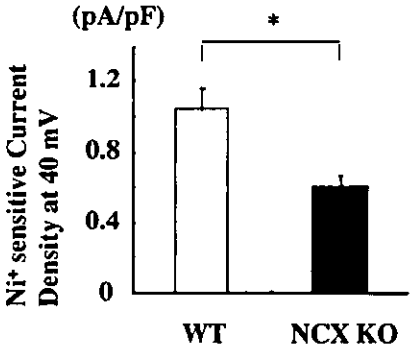

Fig. 1. NCX current densities. The densities of the reverse mode of NCX at 40 mV in ventricular myocytes isolated from WT ($n = 9$) and NCX KO mice hearts ($n = 6$). Values are expressed as means ± SEM. *$p < 0.05$ vs. WT mice.

Mechanical function of hearts before and after ischemia/reperfusion

There were no significant differences in the basal hemodynamic parameters including heart rate, left ventricular pressure, end-diastolic pressure, and positive and negative d*P*/d*t*, between WT and KO mice (Table 1). After ischemia, there was no significant difference between the two groups in several parameters such as time to no beating, time to contracture, and left ventricular end-diastolic pressure (Fig. 2). After reperfusion, however, hearts of KO mice started to beat earlier than those of WT mice (Fig. 2). At 120 min after reperfusion, contractile function (left ventricular developed pressure) of KO mice hearts was significantly better (51.7 ± 12.7% of pre-ischemic value) than that of WT mice hearts (26.3 ± 6.9%, $p < 0.05$) (Fig. 3).

Myocardial infarction after ischemia/reperfusion

After ischemia/reperfusion, there was much viable myocardium in KO hearts than WT hearts (red lesion in Fig. 4A). The infarct size was significantly smaller in KO hearts (32 ± 9%) than in WT hearts (68 ± 10%, $p < 0.05$) (white lesion in Figs. 4A and B).

Table 1
Hemodynamic parameters of NCX KO mice

	WT ($n = 6$)	NCX KO ($n = 7$)
HR(bpm)	356 ± 40	378 ± 77
LVP (mmHg)	142.8 ± 40	146.3 ± 34.5
EDP (mmHg)	4.4 ± 1.5	4.3 ± 1.3
d*P*/d*t* (mmHg/s)	7368 ± 630	7845 ± 2582
−d*P*/d*t* (mmHg/s)	5204 ± 782	5539 ± 1157
Time to no beating (min)	2.2 ± 0.9	2.2 ± 1.6
Time to contracture (min)	6.2 ± 1.7	6.3 ± 2.0
EDP at 25 min (mmHg)	67.3 ± 9.2	63.8 ± 10.8

HR, heart rate; LVP, left ventricular pressure; EDP, LV end-diastolic pressure; d*P*/d*t* and −d*P*/d*t*, positive and negative first derivatives for maximal rates of LV pressure development.

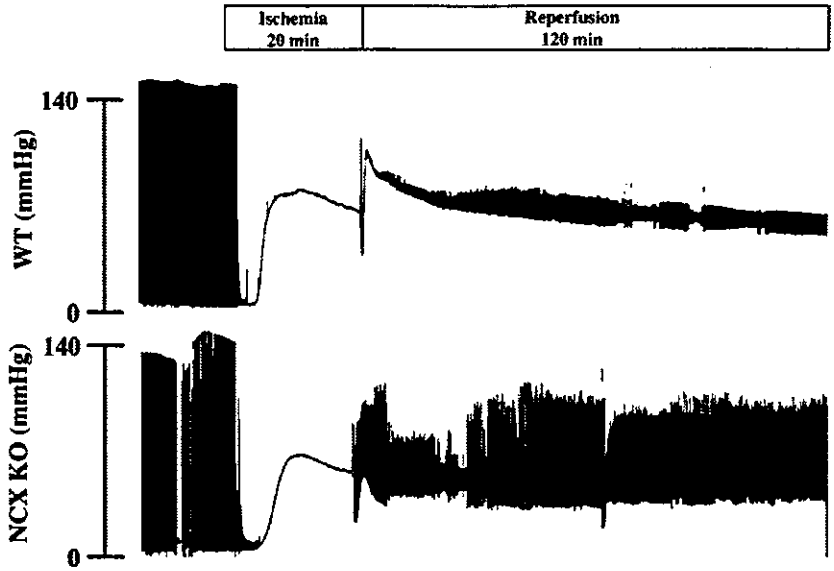

Fig. 2. Ex vivo studies. Changes in LVP during ischemia/reperfusion. Representative LVP records of WT and NCX KO mice hearts are shown. Note that KO mice hearts started to contract earlier than WT mice hearts after reperfusion.

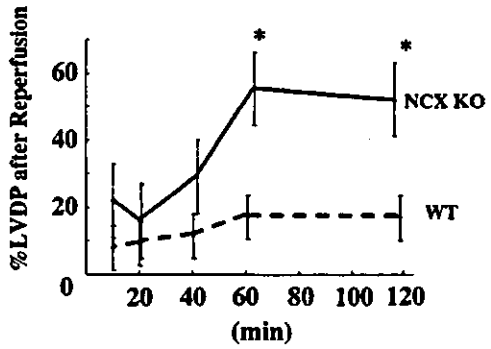

Fig. 3. LVDP of hearts of NCX KO mice ($n = 7$) and WT mice ($n = 6$) hearts after reperfusion. Values are expressed as means ± SEM. $^*p < 0.05$ vs. WT mice.

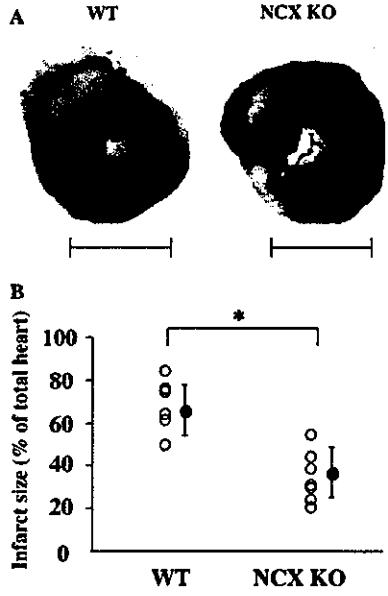

Fig. 4. (A) Representative TTC staining photographs of WT and NCX KO mice hearts after ischemia/reperfusion are shown. Infarcted area is expressed as white lesion and viable myocardium is expressed as red lesion. Bar = 2 mm. (B) Myocardial infarct size is expressed as percentage for total heart of WT mice ($n = 6$) and NCX KO mice ($n = 7$). Values are expressed as means ± SEM. $^*p < 0.05$ vs. WT mice.

Discussion

Myocardial cell injury is induced by a combination of mechanical and chemical stresses during ischemia [14]. Reoxygenation after extended periods of ischemia rapidly induces hypercontracture of cardiomyocytes [15] and aggravates the pre-existing injury [16]. The hypercontracture represents a major cause of acute lethal cell injury in the reperfused myocardium [17,18]. It has been hypothesized that an increase in intracellular Ca^{2+} levels of cardiomyocytes through NCX induces the hypercontracture state after reperfusion but not during ischemia by the mechanism described below [5]. During myocardial ischemia, anaerobic metabolism induces acidosis both inside and outside of cardiomyocytes. The Na^+–H^+ exchanger does not operate at this moment because of no difference in H^+ concentration across the plasma membrane of cardiomyocytes. Reperfusion

restores extracellular acidosis, leading to a disparity in H^+ concentration between inside and outside of cardiomyocytes. The increase in intracellular H^+ concentration activates the Na^+–H^+ exchanger, and the elevated intracellular Na^+ concentration triggers a rise in intracellular Ca^{2+} by the reverse mode of NCX [5]. The excessive Ca^{2+} overload induces the catastrophic hypercontracture of cardiomyocytes. In fact, it has been reported that reduction of Ca^{2+} concentration protects cardiomyocytes against hypercontracture evoked by reoxygenation [19]. In contrast, overexpression of NCX increased ischemia/reperfusion injury in mice [20]. Pharmacological inhibition of reverse mode of NCX protected reperfusion injury in cardiomyocytes [19]. These results suggest that NCX is critically involved in the myocardial ischemia/reperfusion injury, however, NCX inhibitors have been recently reported to be not specific to NCX [6]. Two putative NCX inhibitors, KB-R7943 and SEA0400, depressed the Ca^{2+} transients even in cardiomyocytes of NCX null mice [7]. Although these NCX inhibitors have been reported to suppress the reverse mode but not the forward mode of NCX, the administration of high dose of these inhibitors increased infarct size possibly by inhibition of forward mode of NCX [21]. We here demonstrated an important role of NCX in myocardial ischemia/reperfusion injury by using NCX KO mice. The reverse mode of NCX current in KO mice was decreased to a half of WT mice. Loss of function of NCX is assumed to result in alleviation of Ca^{2+} overload, hypercontracture, and cell death after reperfusion. Our present study clearly indicates that the inhibition of NCX contributes to cardioprotection against myocardial ischemia/reperfusion injury and suggests that specific inhibitors of reverse mode of NCX may be useful to prevent the myocardial ischemia/reperfusion injury.

Acknowledgments

We thank to Y. Reien for the current density analysis and R. Kobayashi, E. Fujita, M. Watanabe, M. Iida, and A. Ohkubo for technical assistance. This work was supported in part by grants from Japanese Ministry of Education, Science, Sports and Culture, and Japan Health Sciences Foundation.

References

[1] D. Schulze, P. Kofuji, R. Hadley, M.S. Kirby, R.S. Kieval, A. Doering, E. Niggli, W.J. Lederer, Sodium/calcium exchanger in heart muscle: molecular biology, cellular function, and its special role in excitation–contraction coupling, Cardiovasc. Res. 27 (1993) 1726–1734.

[2] J.H. Bridge, J.R. Smolley, K.W. Spitzer, The relationship between charge movements associated with I_{Ca} and $I_{Na\text{-}Ca}$ in cardiac myocytes, Science 248 (1990) 376–378.

[3] A.G. Kleber, Resting membrane potential, extracellular potassium activity, and intracellular sodium activity during acute global ischemia in isolated perfused guinea pig hearts, Circ. Res. 52 (1983) 442–450.

[4] J.G. Pilitsis, F.G. Diaz, M.H. O'Regan, J.W. Phillis, Inhibition of Na^+/Ca^{2+} exchange by KB-R7943, a novel selective antagonist, attenuates phosphoethanolamine and free fatty acid efflux in rat cerebral cortex during ischemia–reperfusion injury, Brain Res. 916 (2001) 192–198.

[5] B.N. Eigel, R.W. Hadley, Antisense inhibition of Na^+/Ca^{2+} exchange during anoxia/reoxygenation in ventricular myocytes, Am. J. Physiol. Heart Circ. Physiol. 281 (2001) H2184–H2190.

[6] H. Reuter, S.A. Henderson, T. Han, T. Matsuda, A. Baba, R.S. Ross, J.I. Goldhaber, K.D. Philipson, Knockout mice for pharmacological screening: testing the specificity of Na^+/Ca^{2+} exchange inhibitors, Circ. Res. 91 (2002) 90–92.

[7] K. Wakimoto, K. Kobayashi, O.M. Kuro, A. Yao, T. Iwamoto, N. Yanaka, S. Kita, A. Nishida, S. Azuma, Y. Toyoda, K. Omori, H. Imahie, T. Oka, S. Kudoh, O. Kohmoto, Y. Yazaki, M. Shigekawa, Y. Imai, Y. Nabeshima, I. Komuro, Targeted disruption of Na^+/Ca^{2+} exchanger gene leads to cardiomyocyte apoptosis and defects in heartbeat, J. Biol. Chem. 275 (2000) 36991–36998.

[8] M. Suzuki, R.A. Li, T. Miki, H. Uemura, N. Sakamoto, Y. Ohmoto-Sekine, M. Tamagawa, T. Ogura, S. Seino, E. Marban, H. Nakaya, Functional roles of cardiac and vascular ATP-sensitive potassium channels clarified by Kir 6.2-knockout mice, Circ. Res. 88 (2001) 570–577.

[9] Y. Watanabe, J. Kimura, Inhibitory effect of amiodarone on Na^+/Ca^{2+} exchange current in guinea-pig cardiac myocytes, Br. J. Pharmacol. 131 (2000) 80–84.

[10] J. Kimura, S. Miyamae, A. Noma, Identification of sodium–calcium exchange current in single ventricular cells of guinea-pig, J. Physiol. 384 (1987) 199–222.

[11] Y. Zou, I. Komuro, T. Yamazaki, S. Kudoh, H. Uozumi, T. Kadowaki, Y. Yazaki, Both Gs and Gi proteins are critically involved in isoproterenol-induced cardiomyocyte hypertrophy, J. Biol. Chem. 274 (1999) 9760–9770.

[12] M. Suzuki, N. Sasaki, T. Miki, N. Sakamoto, Y. Ohmoto-Sekine, M. Tamagawa, S. Seino, E. Marban, H. Nakaya, Role of sarcolemmal K(ATP) channels in cardioprotection against ischemia/reperfusion injury in mice, J. Clin. Invest. 109 (2002) 509–516.

[13] E. Takimoto, A. Yao, H. Toko, H. Takano, M. Shimoyama, M. Sonoda, K. Wakimoto, T. Takahashi, H. Akazawa, M. Mizukami, T. Nagai, R. Nagai, I. Komuro, Sodium calcium exchanger plays a key role in alteration of cardiac function in response to pressure overload, FASEB J. 16 (2002) 373–378.

[14] H.M. Piper, D. Garcia-Dorland, M. Ovize, A fresh look at reperfusion injury, Cardiovasc. Res. 38 (1998) 291–300.

[15] B. Siegmund, A. Koop, T. Klietz, P. Schwartz, H.M. Piper, Sarcolemmal integrity and metabolic competence of cardiomyocytes under anoxia-reoxygenation, Am. J. Physiol. 258 (1990) H285–H291.

[16] M.D. Stern, A.M. Chien, M.C. Capogrossi, D.J. Pelto, E.G. Lakatta, Direct observation of the "oxygen paradox" in single rat ventricular myocytes, Circ. Res. 56 (1985) 899–903.

[17] J.A. Barrabes, D. Garcia-Dorado, M. Ruiz-Meana, H.M. Piper, J. Solares, M.A. Gonzalez, J. Oliveras, M.P. Herrejon, J. Soler-Soler, Myocardial segment shrinkage during coronary reperfusion in situ. Relation to hypercontracture and myocardial necrosis, Pflugers Arch. 431 (1996) 519–526.

[18] C.E. Ganote, Contraction band necrosis and irreversible myocardial injury, J. Mol. Cell. Cardiol. 15 (1983) 67–73.

[19] C. Schafer, Y. Ladilov, J. Inserte, M. Schafer, S. Haffner, D. Garcia-Dorado, H.M. Piper, Role of the reverse mode of the Na^+/Ca^{2+} exchanger in reoxygenation-induced cardiomyocyte injury, Cardiovasc. Res. 51 (2001) 241–250.

[20] H.R. Cross, L. Lu, C. Steenbergen, K.D. Philipson, E. Murphy, Overexpression of the cardiac Na^+/Ca^{2+} exchanger increases susceptibility to ischemia/reperfusion injury in male, but not female, transgenic mice, Circ. Res. 83 (1998) 1215–1223.

[21] J. Inserte, D. Garcia-Dorado, M. Ruiz-Meana, F. Padilla, J. Barrabes, P. Pina, L. Agullo, H. Piper, J. Soler-Soler, Effect of inhibition of Na^+/Ca^{2+} exchanger at the time of myocardial reperfusion on hypercontracture and cell death, Cardiovasc. Res. 55 (2002) 739.

Available online at www.sciencedirect.com
SCIENCE DIRECT®
Biochemical and Biophysical Research Communications 314 (2004) 1014–1020
BBRC
www.elsevier.com/locate/ybbrc

Direct measurement of Ca^{2+} concentration in the SR of living cardiac myocytes

Hiroki Kasai,[a,1] Atsushi Yao,[a,1] Tomomi Oyama,[b] Hiroshi Hasegawa,[b] Hiroshi Akazawa,[b] Haruhiro Toko,[b] Toshio Nagai,[b] Koichiro Kinugawa,[a] Osami Kohmoto,[c] Kei Maruyama,[d] Toshiyuki Takahashi,[a] Ryozo Nagai,[a] Atsushi Miyawaki,[e] and Issei Komuro[b,*]

[a] *Department of Cardiovascular Medicine, Graduate School of Medicine, University of Tokyo, Tokyo, Japan*
[b] *Department of Cardiovascular Science and Medicine, Chiba University Graduate School of Medicine, Chiba 260-8670, Japan*
[c] *The Second Department of Medicine, Saitama Medical School, Japan*
[d] *Department of Pharmacology, Saitama Medical School, Japan*
[e] *Laboratory for Cell Function and Dynamics, Advanced Technology Development Center, Brain Science Institute, The Institute of Physical and Chemical Science (RIKEN), Japan*

Received 17 December 2003

Abstract

Although abnormal sarcoplasmic reticulum (SR) Ca^{2+} handling may cause heart failure, there has been no method to directly measure Ca^{2+} concentration in SR ($[Ca^{2+}]_{SR}$) of living cardiomyocytes. We have measured $[Ca^{2+}]_{SR}$ by expressing novel fluorescent Ca^{2+} indicators *yellow cameleon* (YC) 2.1, YC3er, and YC4er in cultured neonatal rat cardiomyocytes. The distribution of YC2.1 was uniform in the cytoplasm, while that of YC3er/YC4er, containing the signal sequence which recruits them to SR, showed reticular pattern and was co-localized with SERCA2a. The treatment with caffeine reversibly decreased the emission ratio (R) in YC3er/YC4er-expressing myocytes, and the treatment with ryanodine and thapsigargin decreased R irreversibly. During the contraction–relaxation cycle, R was changed periodically in the YC2.1- and YC3er-expressing myocytes, but its direction of the change was opposite. These results suggest that YC3er/YC4er were specifically localized and functioned in SR as a $[Ca^{2+}]_{SR}$ indicator. This technique would be useful to understand the function of SR in failing myocardium.
© 2004 Elsevier Inc. All rights reserved.

Keywords: Sarcoplasmic reticulum; Fluorescent Ca^{2+} indicators; Yellow cameleon; Real-time monitoring; Cardiomyocyte; Caffeine; Thapsigargin; SERCA; Heart failure

Ca^{2+} is the primary regulator for the contraction–relaxation cycle in cardiac muscle, and the sarcoplasmic reticulum (SR) is a key organelle for physiological Ca^{2+} regulation in mammalian cardiomyocyte [1]. The accumulation of a small amount of Ca^{2+} in the diad junctions through the voltage dependent L-type Ca^{2+} channels induces a release of large amount of Ca^{2+} from SR through ryanodine receptors by the Ca^{2+}-induced Ca^{2+} release (CICR) mechanism, leading to myocardial contraction.

During relaxation, cytosolic Ca^{2+} concentration ($[Ca^{2+}]_{cyt}$) is decreased by sequestration into SR by the SR Ca^{2+}-ATPase (SERCA) or efflux from the cytosol by Na^+/Ca^{2+} exchanger (NCX) [2]. Dysfunction of the Ca^{2+} handling proteins of SR has recently been focused as one of the critical factors to cause heart failure [3–6]. Therefore, direct and precise measurement of the intra-SR Ca^{2+} concentration ($[Ca^{2+}]_{SR}$) in living cardiomyocyte is a prerequisite for understanding a molecular link between SR functions and heart failure. Since the kinetics of $[Ca^{2+}]_{SR}$ have been obtained from calculations based on many complicated assumptions such as Ca^{2+} buffering capacity of SR, SR volume, ionic strength, and performance of SERCA, and ryanodine receptors

* Corresponding author. Fax: +81-43-226-2557.
E-mail address: komuro-tky@umin.ac.jp (I. Komuro).
[1] These authors equally contributed to this work.

0006-291X/$ - see front matter © 2004 Elsevier Inc. All rights reserved.
doi:10.1016/j.bbrc.2003.12.189

[7–10], $[Ca^{2+}]_{SR}$ transient during every contraction–relaxation cycle has been only speculated. Recently, we have developed Ca^{2+} sensitive proteins yellow cameleons (YC) [11]. Among YC, YC3er, and 4er have the signal sequence which recruits them into the endoplasmic reticulum (ER), and reflect Ca^{2+} concentration in ER ($[Ca^{2+}]_{ER}$) in response to various stimulations in living non-muscle cells. So we have examined the real-time change of $[Ca^{2+}]_{SR}$ in living ventricular myocytes using YC3er and 4er.

Methods

This investigation conformed to the Guide for the Care and Use of Laboratory Animals (Washington, DC: Natl. Acad. Press, 1996).

Cell culture. Primary cultures of cardiac myocytes were prepared from ventricles of 1-day-old neonatal Wistar rats [12]. In brief, cells enzymatically dissociated from the ventricles were plated at a field density of 1×10^5 cells/cm^2 on 25×50 mm of collagen-coated coverslips in culture medium (Dulbecco's modified Eagle's medium with 10% fetal bovine serum). Twelve hours after seeding, the culture medium was changed to the medium with 0.5% fetal bovine serum.

Constructs of yellow cameleons. Plasmids containing YC2.1, YC3er, and YC4er were described previously [13]. YC3er and YC4er have a mutation of E104Q and E31Q, respectively, which is important for determination of the dissociation constant (K_d value). They also have the calreticulin leading sequence in the N terminus and the retention signal (KDEL) in the C terminus to introduce and detain these products in ER, respectively.

Transfection procedure of cameleon expression vectors. Twelve hours after plating the cells on coverslips, plasmid DNA of each cameleon was transfected using FuGENE6 (Roche, Basel, Switzerland). One microgram of DNA mixed with 3 μl of FuGENE6 reagent was added in the culture medium. The transfection efficiency of each experiment was ~5%, as determined by counting the number of cells which had significant emission of 530 nm-fluorescence excited by 420 ± 20 nm-light.

Staining of SR Ca^{2+}-ATPase (SERCA) 2a and actin filaments. After the transfection procedure, the cells were fixed with 4% paraformaldehyde-containing PBS and then permeated by 0.2% Triton X-contained PBS. For the immunostaining of SERCA2a, the cells were blocked with 5% fetal calf serum-contained PBS, incubated with affinity-purified monoclonal anti-SERCA2a antibodies (Affinity Bioreagents), and subsequently incubated with secondary fluorescein-conjugated anti-mouse IgG antibodies (CHEMICON, Temecula, USA). For the staining of the actin filaments, the permeated cells were stained with TRITC-labeled phalloidin (Sigma-Aldrich, St. Louis, USA).

Confocal images. Images were obtained using a confocal laser scanning microscopy system equipped with argon-laser and an acousto-optic tunable filter (Leica, Wetzlar, Germany). To obtain the fluorescence images from the cameleons and fluo-3, cells were excited at a wavelength of 488 nm and the emission light of 500–535 nm was acquired. The loading of fluo-3 was performed as described previously [14]. For the images of SERCA2a and actin filaments, cells were excited at 543 nm and then the emission light at 555–700 nm was acquired.

Measurement of $[Ca^{2+}]_{cyt}$ and $[Ca^{2+}]_{SR}$. The measurement of Ca^{2+} concentration was carried out with a modification of the method used for indo-1 [15]. In brief, cells were perfused with Hepes solution (126 mM NaCl, 4.4 mM KCl, 1.0 mM $MgCl_2$, 13 mM NaOH, 1.08 mM $CaCl_2$, 11 mM glucose, and 24 mM Hepes, adjusting pH to 7.4 at 25 °C) at a constant flow rate ($\geqslant$ 2 ml/min) in a heated chamber (24–6 °C) which was equipped on the stage of an inverted epifluorescence microscope (Nikon Diaphot). A myocyte expressing YC could be selected by the image of emission fluorescence passing through the dichroic mirror (DM455, Nikon), and non-myocytes having YCs fluorescence could be screened out because they did not contract in response to pacing stimulation. The myocyte within the field was then excited with the light from a 100 W mercury-arc lamp (Nikon) passing through a 420 ± 20 nm band pass filter (BV-2A, Nikon), and an emission fluorescence was detected simultaneously at 480 (BA, Nikon) and 530 nm (DF30, Omega) with a photomultiplier tube (PMT; model 1897 AH, Hamamatsu). The fluorescence of the optical field without YCs positive cells was measured as zero.

Data analysis. The emission signals from the YCs were digitized using a Digidata1200A analog-to-digital converter (Axon Instruments) and stored in a personal computer (Gateway). The data were analyzed with Axoscope1.0 (Axon Instruments) and Origin4.0 (Microcal) software.

Results

Expressing pattern of cameleons

YC2.1, YC3er, and YC4er were successfully expressed in cultured neonatal rat ventricular myocytes (Fig. 1). The protein of YC2.1 was localized in the cytosol in a homogeneous pattern except for the space probably occupied by intra-cellular organelles (Fig. 1A). As compared with the conventional Ca^{2+} sensitive dye fluo-3 (Fig. 1B), expression of YC2.1 was spared in the nucleus, suggesting that expression of YC2.1 is localized in the cytoplasm of cardiomyocytes. In contrast, YC3er showed fine reticular expression pattern around the nucleus and a ladder-like pattern in the peripheral region of cardiomyocytes (Fig. 1C). Immunocytochemisty using TRITC-labeled phalloidin revealed that the parallel lines of fine reticular region corresponded to the middle of actin filaments (I bands) (Figs. 1D–F), where there are diad junctions. Since these results suggest that YC3er is localized in SR, we examined the co-localization of YC3er and the SR protein SERCA2a. The expression pattern of YC3er was very similar to that of SERCA2a (Figs. 1G–I). The distribution of YC4er was also similar to that of YC3er (data not shown). Co-localization of YC3er and YC4er with SERCA2a at I bands suggests that YC3er and YC4er were located in SR membranes.

Ca^{2+} transient measured by cameleons

To evaluate the dynamics of intra-cellular Ca^{2+} transient, the emitted fluorescences of 480 and 530 nm from cameleons excited by 420 ± 20 nm-light were simultaneously recorded, and the ratio of 530- to 480 nm-intensity (R) was calculated. In the YC2.1-expressing myocyte, the end diastolic R was continuously raised by pacing (0.5 Hz) (Fig. 2a), and beat-to-beat oscillated R transient was seen during each contraction–relaxation cycle (Fig. 2a-A), which was quite similar to the signal monitored by use of conventional Ca^{2+} sensitive dyes

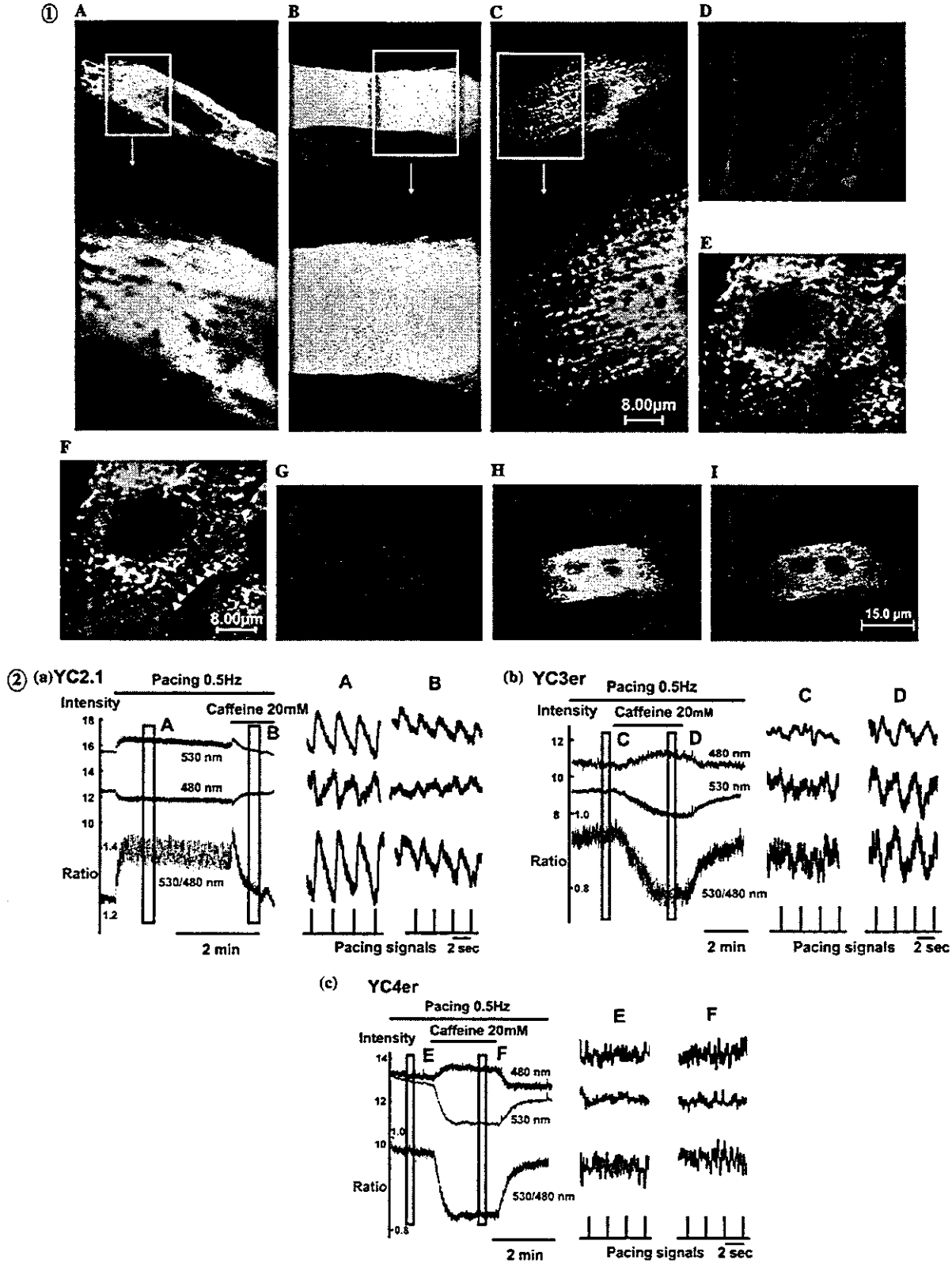
①
A
B
C
D
E
F
G
H
I
8.00μm
8.00μm
15.0 μm
② (a)YC2.1
Pacing 0.5Hz
Intensity
Caffeine 20mM
530 nm
480 nm
530/480 nm
Ratio
2 min
Pacing signals
2 sec
(b) YC3er
Pacing 0.5Hz
Intensity
Caffeine 20mM
480 nm
530 nm
530/480 nm
Ratio
2 min
Pacing signals
2 sec
(c) YC4er
Pacing 0.5Hz
Intensity
Caffeine 20mM
480 nm
530 nm
530/480 nm
Ratio
2 min
Pacing signals
2 sec

Fig. 1. Confocal fluorescence images of YC2.1, YC3er-, and YC4er-expressing cells. (A) In the YC2.1-expressed myocyte, emitted fluorescence of 530 nm was uniform in the cytosol without any significant brighter spot. Fluorescence was spared in the nucleus. (B) In the fluo-3-loaded myocyte, the fluorescence of 530 nm was homogeneous in the cytosol and intra-cellular organelles with some brighter spots. (C) The image of the YC3er-expressed myocyte showed reticular pattern around the nucleus and a ladder-like pattern in the peripheral lesion of the myocyte. The YC4er-expressing myocyte (E) was simultaneously stained with TRITC-labeled phalloidin (D). The parallel lines (arrowheads) of YC4er-expressing region were located in the middle of the I bands (Merge, (F)). Note that the distance between the neighbored cross-sectional parallel lines was about 2 μm. Simultaneous detection of distribution of SERCA2a (G) and YC3er (H) was performed using confocal laser microscopy. The distribution of YC3er was overlapped with the expression pattern of SERCA2a (Merge, (I)).

Fig. 2. Ca^{2+}-dependent FRET signals from the YC2.1, YC3er-, and YC4er-expressing ventricular myocytes. In the YC2.1-expressing myocyte, the emission signals of 480 nm (black line) were decreased and the signals of 580 nm (red line) were increased by pacing stimulation (a). As a result, calculated *R* (blue line) was transiently increased during each contraction–relaxation cycle (A), and the rapid application of caffeine (20 mM) decreased both the diastolic and the amplitude of *R* (B) after transiently increasing the diastolic level of *R*. In the YC3er-expressed myocyte, *R* was reversibly decreased by caffeine (b). The beat-to-beat oscillation of the emission lights was observed after the caffeine-treatment (D) but not before the treatment (C). In the YC4er-expressed myocyte, *R* was decreased by caffeine-like in the YC3er-expressing myocyte (c), but the beat-to-beat oscillation was not observed with (F) or without (E) the treatment.

[16,17]. Treatment with 20 mM of caffeine initially and transiently increased the baseline (diastolic level) of *R*, resulting from an increase in the 530 nm-emission intensity and a decrease in the 480 nm-emission intensity, which was followed by a decrease in that of *R* with reduction in the amplitude of *R* transients (Fig. 2a-B). These results suggest that YC2.1 was localized in the cytosol and reflected a change in the cytosolic Ca^{2+} concentration ($[Ca^{2+}]_{cyt}$) during each contraction–relaxation cycle. In the YC3er-expressing myocyte, the emission of both 480 and 530 nm did not change synchronously by pacing stimulations (Fig. 2b-C). In contrast to YC2.1, the emission of 480 nm was increased and that of 530 nm was decreased by treatment with 20 mM of caffeine (Fig. 2b-D). A beat-to-beat periodical *R* transient was detected during the caffeine treatment and the phase of the *R* transient was completely inverted to that observed in the YC2.1-expressing myocyte (Figs. 2a-B and b-D). *R* was increased soon after pacing stimulation in the YC2.1 expressing myocyte (Fig. 2a), while *R* was peaked at pacing stimulation and decreased thereafter in the YC3er-expressing myocytes (Fig. 2b). In the YC4er-expressing myocyte, *R* was decreased by the treatment with caffeine (Fig. 2c), but periodical transient was not observed before and after caffeine treatment (Fig. 2c-E and F). Since caffeine induces efflux of Ca^{2+} from SR and we have confirmed that caffeine of this high concentration did not alter the emission signals from cardiac fibroblasts expressing YC3er or YC4er as well as HEK293 cells expressing YC2.1 (data not shown), the results of caffeine treatment suggest that change in the emission signals from YC3er and YC4er can be considered to be Ca^{2+}-dependent, that is, reflect the change in $[Ca^{2+}]_{SR}$.

Change of $[Ca^{2+}]_{SR}$

Next we examined the effects of Ca^{2+} modulating agents such as isoproterenol, thapsigargin, and ryanodine on *R*. Isoproterenol has been known to increase Ca^{2+} influx through L-type Ca^{2+} channels of sarcolemma, leading to an increase in large Ca^{2+} release from SR by the CICR mechanism. Isoproterenol also increases the pumping rate of SERCA2a by phosphorylating phospholamban through Gs protein-coupled protein kinase A activation. Addition of 100 nM isoproterenol increased *R* in the YC4er- and YC3er-expressing myocytes (Fig. 3A, data not shown). Thapsigargin has been widely used as an inhibitor for SERCA2a. As shown in Fig. 3B, 10μM of thapsigargin decreased *R* in the YC4er-expressing myocyte, which was not reversed after removal of thapsigargin from the perfusate. Subsequent application of caffeine further decreased *R* and this reduction was reversed soon

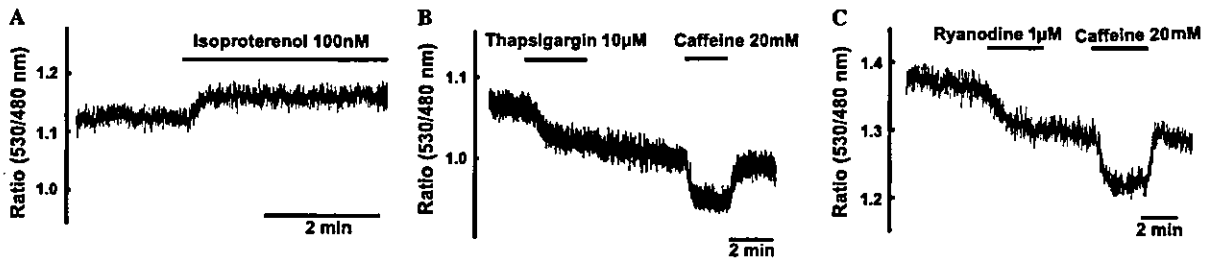

Fig. 3. Effects of isoproterenol, thapsigargin, and ryanodine on $[Ca^{2+}]_{SR}$. Treatment with 100 nM of isoproterenol increased *R* in the YC4er-expressed myocyte. (A) On the other hand, 10 μM of thapsigargin (B) or 1 μM of ryanodine (C) irreversibly decreased *R* in the YC4er-expressing myocyte and subsequent treatment with caffeine (20 mM) further decreased *R* reversibly.

after the end of caffeine treatment (Fig. 3B). Ryanodine at the concentration of 1 μM has been reported to increase the open probability of SR Ca^{2+} channel (ryanodine receptor) and consequently decrease $[Ca^{2+}]_{SR}$. As shown in Fig. 3C, the ryanodine treatment decreased R irreversibly and the subsequent application of caffeine further decreased R. Similar results were obtained in YC3er-expressing myocytes (data not shown).

Discussion

In the present study, we succeeded in specifically expressing YC2.1 in the cytoplasm and YC3er/4er in SR of living ventricular myocytes, and established the method for measuring $[Ca^{2+}]_{cyt}$ and $[Ca^{2+}]_{SR}$. The validity of the method for measuring $[Ca^{2+}]_{SR}$ was confirmed by the reverse directions of Ca^{2+} transient observed in YC2.1 expressing myocytes and YC3er-expressing myocytes during pacing and by the effects of isoproterenol, thapsigargin, and ryanodine on Ca^{2+} concentration in YC4er- and YC3er-expressing myocytes.

Intra-cellular distribution of cameleons

YC2.1 was expressed homogeneously in the cytoplasm, whereas YC3er and YC4er showed a characteristic expression pattern in ventricular myocytes. Expression of YC2.1 was spared in the nucleus or the intra-cellular organelles. Since molecular size of cameleons is relatively large (74 kDa), they could not get into those organellae. In contrast, conventional Ca^{2+} dyes can be taken by organellae such as mitochondria and Golgi apparatus as well as the nucleus. The cytosolic homogeneous pattern of YC2.1 also suggests that YC2.1 resides in the fluid space of the cytosol without accumulation or binding to hydrophobic proteins, which is consistent with results in non-muscle cells [11]. The specific localization and the uniform distribution give the priority to the YCs as a Ca^{2+} indicator as compared with conventional fluorescence indicators such as fura-2, indo-1, and fluo-3.

In mature ventricular myocytes, it has been reported that calsequestrin is a major protein to buffer Ca^{2+} in SR and is predominantly (60–70%) expressed in the terminal cisternae [18–20], while calreticulin composes a minor part [21]. YC3er and YC4er possess the leading sequence and the retention signal (KDEL) of calreticulin, which introduce and detain these cameleons in the ER of nonmyocytes [11]. YC4er was located in the middle of I-bands (Figs. 1D–F), suggesting that YC4er was expressed in the part of the terminal cisternae. Immunocytochemical analysis using anti-SERCA2a antibody indicated that YC3er and YC4er were localized in the same place as SERCA2a (Fig. 1H). These results suggest that YC3er and YC4er were expressed in terminal cisternae of SR.

$[Ca^{2+}]_{SR}$ transients

Although the relatively slow changes in $[Ca^{2+}]_{SR}$ were observed after several manipulations (Fig. 3), we could not observe the cyclic emission signals which were synchronized with beating in the YC3er/4er-expressing myocyte. Since treatment with caffeine unraveled beat-to-beat oscillated R in the YC3er-expressing cells, the limited speed of the Ca^{2+}-dependent conformational change of YC3er is not a major cause of irresponsiveness to pacing stimulations. The difference in beat-to-beat oscillation after caffeine treatment between YC3er and YC4er (Figs. 2b and c) suggests that the irresponsiveness might be at least in part due to dissociation constant (K_d). K_d of YC3er has been reported to be 4.4 μM at 25 °C [11,13]. In the earlier reports [10,22–24], $[Ca^{2+}]_{SR}$ has been reported to be 0.3–5 mM, the range of which is much higher than the K_d value for YC3er. Therefore, YC3er may be saturated with Ca^{2+} and it cannot follow the change in $[Ca^{2+}]_{SR}$. This interpretation seems to be reasonable, because the emission signals from YC3er actually showed beat-to-beat transients in response to pacing when Ca^{2+} in SR was reduced by caffeine. However, beat-to-beat signals were not detected from YC4er-expressing cardiomyocyte in response to pacing stimulation even after the caffeine treatment, suggesting that there are other reasons. The first possibility is that YC4er was expressed so much that YC4er itself buffered Ca^{2+} in SR as suggested previously [11,13], resulting in suppression of CICR and/or secondary modification of Ca^{2+} handling systems consisting of L-type Ca^{2+} channel, ryanodine receptors, the dyadic or triadic structure, and so on. In fact, the $[Ca^{2+}]_{cyt}$ transients were markedly reduced when the intra-SR buffering capacity was much increased by overexpression of calsequestrin, although the total Ca^{2+} content in SR was markedly increased [25,26]. The second possibility is that the intra-SR Ca^{2+} concentration may be out of the measurable range with YC3er and YC4er in neonatal rat ventricular myocytes. The Ca^{2+} titration curve for YC4er has been reported to be a biphasic sigmoid curve with rather linear relationship at 10^{-4}–10^{-2} M of Ca^{2+} concentration. This suggests that YC4er could not be used as a Ca^{2+} indicator in the range of Ca^{2+} concentrations below 10^{-4} M or above 10^{-2} M. On the other hand, the titration curve for YC3er has been reported to be well fitted with a single sigmoid curve with almost linear relationship between 10^{-7} and 10^{-5} M [11]. Therefore, resting $[Ca^{2+}]_{SR}$ might be 10^{-5}–10^{-4}. We could not achieve the calibration, because of deformation and rigor of cardiomyocytes when we increased $[Ca^{2+}]_{cyt}$ up to more than 10^{-2} M with ionomycin. Furthermore, both YC3er and YC4er did not

respond to high $[Ca^{2+}]_{SR}$ ($\geqslant 10^{-2}$ M) solution in the presence of ionomycin (data not shown), suggesting that the cell damage might affect the conditions of YC3er and YC4er in the SR. Further studies are necessary to establish precise calibration to use these cameleons for general measurements of $[Ca^{2+}]_{SR}$ in cardiac myocytes.

$[Ca^{2+}]_{SR}$ after addition of Ca^{2+} modulating agents

Although cameleons could not follow the rapid change of $[Ca^{2+}]_{SR}$, they could respond to the relatively slow and large change in $[Ca^{2+}]_{SR}$. Isoproterenol increased R in cardiac myocytes expressing YC4er and YC3er (Fig. 3A). Ten micromolars of thapsigargin has been widely used to diminish the pumping rate of SERCA2a, and has been reported to deplete SR Ca^{2+} content almost irreversibly because of its high affinity [27]. As shown in Fig. 3B, thapsigargin decreased R irreversibly. However, the subsequent application of caffeine further and reversibly decreased R, suggesting that the treatment with 10 μM of thapsigargin for 3 min is not enough to inhibit SERCA2a completely or to deplete Ca^{2+} storage in SR. Ryanodine at 1 μM has been thought to set the ryanodine receptor subconducting state [28], which likely accelerates the leak of Ca^{2+} from SR, and reduces $[Ca^{2+}]_{SR}$. As shown in Fig. 3C, ryanodine decreased R in the YC4er-expressing myocyte. The effect by subsequent application of caffeine was maintained, suggesting that ryanodine partially releases a part of Ca^{2+} in SR.

The effect of caffeine at the concentration of this range (20 mM) has been well recognized to set the ryanodine receptor subconducting state and prevent net SR Ca^{2+} reuptake [29], both of which result in Ca^{2+} release from SR and the depletion of releasable Ca^{2+} in SR. Therefore, the beat-to-beat $[Ca^{2+}]_{cyt}$ oscillation induced by pacing in the presence of caffeine has been thought to be mediated by Ca^{2+} influx through L-type Ca^{2+} channels and reverse phase of NCX. In this study, however, CICR was detectable by cameleons even after the caffeine treatment. Caffeine has been reported to inhibit phosphodiesterases to increase cAMP, thereby activating SERCA as well as further increasing I_{Ca} through protein kinase A-dependent mechanism, both of which may contribute to maintaining the amount of releasable Ca^{2+} in SR. Reconsideration may be necessary for the effects of caffeine on Ca^{2+} regulation in cardiomyocytes, although it is not ruled out that difference in species, age, and experimental conditions might contribute to this intricate effect of caffeine.

In conclusion, we for the first time succeeded in monitoring the real-time changes of $[Ca^{2+}]_{SR}$ in living ventricular myocytes expressing novel Ca^{2+} indicators, YC3er and YC4er. We also examined the effects of drugs which modify the function of SR Ca^{2+} handling proteins such as SERCA2a and ryanodine receptors. Although the calibration of emission signals to Ca^{2+} concentration has not be established, this technique is useful and applicable to evaluate the $[Ca^{2+}]_{SR}$ in cardiomyocytes of pathological and various pathophysiological conditions.

Acknowledgments

This work was partly supported by a Grant-in-Aid for Scientific Research on Priority Areas from the Ministry of Education, Culture, Sports, Science and Technology of Japan, Japan Heart Foundation, Takeda Medical Research Foundation, Uehara Memorial Foundation, and Grant-in-Aid of Japan Medical Association, The Kato Memorial Trust for Nambyo Research, and Takeda Science Foundation. We thank Dr. Makoto Endo and Dr. William. H. Barry for their kind suggestions on the experimental protocols and the results in this study.

References

[1] D.M. Bers, Cardiac excitation–contraction coupling, Nature 415 (2002) 198–205.
[2] W.H. Barry, J.H. Bridge, Intracellular calcium homeostasis in cardiac myocytes, Circulation 87 (1993) 1806–1815.
[3] R. Studer, H. Reinecke, J. Bilger, T. Eschenhagen, M. Bohm, G. Hasenfuss, H. Just, J. Holtz, H. Drexler, Gene expression of the cardiac Na(+)–Ca^{2+} exchanger in end-stage human heart failure, Circ. Res. 75 (1994) 443–453.
[4] M. Meyer, W. Schillinger, B. Pieske, C. Holubarsch, C. Heilmann, H. Posival, G. Kuwajima, K. Mikoshiba, H. Just, G. Hasenfuss, Alterations of sarcoplasmic reticulum proteins in failing human dilated cardiomyopathy, Circulation 92 (1995) 778–784.
[5] S. Minamisawa, M. Hoshijima, G. Chu, C.A. Ward, K. Frank, Y. Gu, M.E. Martone, Y. Wang, J. Ross Jr., E.G. Kranias, W.R. Giles, K.R. Chien, Chronic phospholamban–sarcoplasmic reticulum calcium ATPase interaction is the critical calcium cycling defect in dilated cardiomyopathy, Cell 99 (1999) 313–322.
[6] S.O. Marx, S. Reiken, Y. Hisamatsu, T. Jayaraman, D. Burkhoff, N. Rosemblit, A.R. Marks, PKA phosphorylation dissociates FKBP12.6 from the calcium release channel (ryanodine receptor): defective regulation in failing hearts, Cell 101 (2000) 365–376.
[7] J.W. Bassani, R.A. Bassani, D.M. Bers, Twitch-dependent SR Ca accumulation and release in rabbit ventricular myocytes, Am. J. Physiol. 265 (1993) C533–C540.
[8] D.A. Eisner, H.S. Choi, M.E. Diaz, S.C. O'Neill, A.W. Trafford, Integrative analysis of calcium cycling in cardiac muscle, Circ. Res. 87 (2000) 1087–1194.
[9] A.W. Trafford, M.E. Diaz, D.A. Eisner, A novel, rapid and reversible method to measure Ca buffering and time-course of total sarcoplasmic reticulum Ca content in cardiac ventricular myocytes, Pflugers Arch. 437 (1999) 501–503.
[10] W. Hasselbach, H. Oetliker, Energetics and electrogenicity of the sarcoplasmic reticulum calcium pump, Annu. Rev. Physiol. 45 (1983) 325–339.
[11] A. Miyawaki, J. Llopis, R. Heim, J.M. McCaffery, J.A. Adams, M. Ikura, R.Y. Tsien, Fluorescent indicators for Ca^{2+} based on green fluorescent proteins and calmodulin, Nature 388 (1997) 882–887.
[12] P. Simpson, A. McGrath, S. Savion, Myocyte hypertrophy in neonatal rat heart cultures and its regulation by serum and by catecholamines, Circ. Res. 51 (1982) 787–801.
[13] A. Miyawaki, O. Griesbeck, R. Heim, R.Y. Tsien, Dynamic and quantitative Ca^{2+} measurements using improved cameleons, Proc. Natl. Acad. Sci. USA 96 (1999) 2135–2140.